

UNCLASSIFIED

AD NUMBER

AD483686

LIMITATION CHANGES

TO:

Approved for public release; distribution is unlimited.

FROM:

Distribution authorized to U.S. Gov't. agencies and their contractors;
Administrative/Operational Use; 15 MAR 1966.
Other requests shall be referred to Air Force Office of Scientific Research, Washington, DC 20333.

AUTHORITY

afosr ltr, 12 nov 1971

THIS PAGE IS UNCLASSIFIED

AFOSR 66-0885

Final Scientific Report | January 1, 1965 - December 31, 1965

483686

**RESPONSE OF A BURNING PROPELLANT
SURFACE TO EROSION TRANSIENTS**

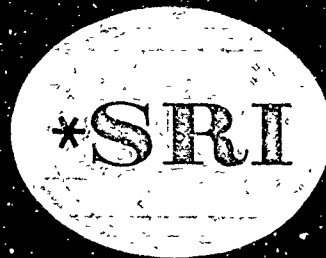
Prepared for:

AIR FORCE OFFICE OF SCIENTIFIC RESEARCH
WASHINGTON, D.C. 20333

CONTRACT AF 49(638)-1507

STANFORD RESEARCH INSTITUTE

MENLO PARK, CALIFORNIA



STANFORD RESEARCH INSTITUTE

MENLO PARK, CALIFORNIA



March 15, 1966

Final Scientific Report

January 1, 1965 - December 31, 1965

RESPONSE OF A BURNING PROPELLANT SURFACE TO EROSION TRANSIENTS

Prepared for:

AIR FORCE OFFICE OF SCIENTIFIC RESEARCH
WASHINGTON, D.C. 20333

CONTRACT AF 49(638)-1507

By: E. L. CAPENER L. A. DICKINSON R. J. KIER G. A. MARXMAN

SRI Project FRU-5458

Approved: LIONEL A. DICKINSON, DIRECTOR
POLYMER & PROPULSION SCIENCES

Copy No. 24

CONTENTS

FOREWORD	iii
LIST OF ILLUSTRATIONS.	vii
LIST OF TABLES	ix
I INTRODUCTION AND SUMMARY	1
II RESEARCH OBJECTIVES.	5
III EXPERIMENTAL AND THEORETICAL PROGRAM	7
A. General.	7
B. Test Instrumentation	8
C. Rocket Motor Configuration	9
D. Propellants Investigated	9
E. Theoretical Studies - Combustion Models.	15
F. Scaling Studies.	16
IV. EXPERIMENTAL RESULTS	17
A. Propellant Compositional Influence	17
1. Composite Propellants--Rocket Motor Studies.	17
2. Monopropellant Combustion of AP.	20
3. Double-Base Propellants--Rocket Motor Studies.	29
B. Combustion Models.	31
1. Theoretical Studies.	31
2. Assumptions and Limitations of Quasi-Steady Analyses of Combustion Extinguishment	32
3. Response of Sinusoidal Pressure Oscillations or an Exponential Pressure Decay; a Stability Criterion.	36
4. Pressure Decay Gradient and Combustion Termination	38
C. Theoretical Relation of Stability Criterion to Motor Pressure and Propellant Linear Burning Rate.	42
D. Experimental Studies to Correlate Stability Criteria With Ballistic Design Parameters and Propellant Micro- structures	45
1. Influence of Fuel/Binder Characteristics on Instability.	49
2. Loss and Gain Processes During Axial Mode Traveling Wave Instability	50

CONTENTS (Concluded)

E. Data Reduction	51
F. Data Interpretation	58
V SUMMARY DISCUSSION	65
A. Compositional Factors	65
B. Composite Propellants	65
C. Double-Base Propellants	68
D. Stability and Scaling	69
E. Analytical Models	69
VI CONCLUSIONS AND FUTURE WORK	71
ACKNOWLEDGEMENT	71
NOMENCLATURE	73
REFERENCES	77
Appendix A SIMPLIFIED MODEL OF UNSTEADY COMBUSTION IN SOLID PROPELLANTS	A-1
Appendix B REFLECTION OF TRAVELING PRESSURE WAVES AT THE ENDS OF THE COMBUSTION CHAMBER	B-1

LIST OF ILLUSTRATIONS

Fig. 1	Instrumentation Block Diagram.	8
Fig. 2	5-Inch X 40-Inch Unstable Combustion Motor Assembly. . .	11
Fig. 3	Opposed Slab Grain for 5-Inch Diameter Motors, , , . . .	13
Fig. 4	Typical Propellant Burning Rate Curves Relative to Stability Bound Found for Propellants Containing Ammonium Perchlorate	18
Fig. 5	Propellant Burning Rate Data for Propellants PU 125M and PU 127	19
Fig. 6	(a) Performance Curve Pressure vs. Time for AP/AN Propellant (PU 127) Showing Ballistic Behavior on Pulsing.	21
	(b) Oscilloscope Playback Record of Second Pulse Showing Over-All Pressure Response During 300-msec Pressure Excursion	21
	(c) High Response Oscilloscope Playback Showing Growth and Data of Axial Instability During the Growth of the Pressure Excursion	21
Fig. 7	40-Inch-Long Acoustic Burner Fitted With Infrared Viewing Port and Pressure Transducers.	23
Fig. 8	Schematic Layout of Infrared Radiation Detection Device :	25
Fig. 9	(a and b) Pressure Oscillations Observed During Unstable Burning of Pressed Ammonium Perchlorate Pellets.	26
Fig. 10	(a) Oscillations in Pressure and Infrared Radiation Observed During the Burning of Pressed Ammonium Perch- lorate Pellets (Test 63)	27
	(b) Pressure/Time Trace, D.C. and A.C. Coupled, Obtained During Combustion of Pressed Ammonium Perch- lorate Pellets	27
Fig. 11	Summary of Instability Data for Two Representative Double-Base Propellants, Showing Stable Operation at Elevated Pressures.	30
Fig. 12	Time Dependence of Burning Rate Derivatives.	39
Fig. 13	Predicted Stability Bounds for Pressure-Sensitive Surface Reactions.	44
Fig. 14	Predicted Stability Bounds for Pressure-Insensitive Surface Reactions.	44

LIST OF ILLUSTRATIONS (Concluded)

Fig. 15	Stability Bound for 40-Inch and 80-Inch Long Motors. . .	47
Fig. 16	Burning Rate and Stability Data for Propellants With Matched Ballistics but Different Oxidizer Particle Size. . .	48
Fig. 17	Schematic Layout and Data Analysis Procedure for Axial Station Probing of Traveling Waves in Rocket Motors. . .	50
Fig. 18	Observed Peak Pressure Amplitude of the Traveling Wave During Propagation in a 5-Inch Dia. X 80-Inch-Long Rocket Motor Burning PBAN 103.	53
Fig. 19	(a) Observed Peak Pressure Amplitude as a Function of Motor Through (d) Length During Transit Up and Down the Motor	
	(a) 24-Inch Motor	54
	(b) 40-Inch Motor	54
	(c) 40-Inch Motor	55
	(d) 80-Inch Motor	55
Fig. 20	Traveling Wave Pressure Time History for 40-Inch Motor at Various Time Intervals.	56
Fig. 21	Multi-Station Pressure Response Observed in a 15-Inch Motor on Pulsing ,	58
Fig. 22	Normalized Growth Characteristics for Traveling Waves Observed in Rocket Motors of Different Lengths	59
Fig. 23	Typical Oscillogram Used for Computation of the Velocity of the Traveling Wave in the 80-Inch Long Rocket Motor	60
Fig. 24	Velocity Profile of Traveling Wave as Determined by Arrival Time of Wave at Pressure Transducers	62
Fig. 25	Visualization of Phase Relationship Between Pressure and Velocity of a Traveling Wave in 80-Inch Long Rocket Motor	63
Fig. 26	Influence of Burning Rate and Composition on Finite Amplitude Traveling Wave Instability; Solid Line Stable Regime, Dotted Line Unstable Regime for 5-Inch X 40-Inch Motor.	66
 APPENDIX A		
Fig. A-1	Combustion Model With Gas Phase and Solid Phase Reaction.	A-2
 APPENDIX B		
Fig. B-1	(a) Visualization of Shock Wave Structure Behind Traveling Shock Front in Rocket Motor	B-2
	(b) Visualization of Transducer Response,	B-2

LIST OF TABLES

Table I	Propellant Formulations Investigated	
	A. Composite Propellants.	14
	B. Double-Base Propellants.	14
Table II	Propellant Burning Data.	15
Table III	Summary of Experimental Data Relating to Traveling Wave Propagation in Rocket Motors of Varying Lengths .	52

I INTRODUCTION AND SUMMARY

Combustion instability associated with solid rocket propellants has, in recent years, been recognized to arise from the coupling of the physical and chemical processes at or near the surface of the burning propellant with acoustic waves. These waves are often of finite amplitude, and their characteristic frequencies are defined by the geometry of the acoustic cavities (usually the grain port dominates the cavity geometry). The many distinct experimental and developmental programs in acoustic burners and rocket motors have resulted in instability being arbitrarily categorized on a phenomenological basis into several distinct types; these are:

1. High frequency transverse mode acoustic instability
2. Intermediate longitudinal mode acoustic instability
3. Finite amplitude longitudinal traveling wave instability
4. Low frequency or sub-acoustic instability.

It is significant that potentially unstable propellants usually exhibit all types of instability, while other propellants appear to be completely free from instability. Our previous studies showed specifically that inclusion of ammonium perchlorate in composite propellants led to increased susceptibility to transverse and axial type instability; contrariwise it appeared that propellants based on potassium perchlorate, lithium perchlorate, and ammonium nitrate were stable (historically, motor development data also confirm this). In our prior work it was not possible to unequivocally decide whether instability was associated with the over-all ballistic properties of the propellant or with the chemical processes occurring in the combustion wave, because both homogeneous (double-base) and composite propellants burning in certain pressure-burning rate regimes exhibit instability of various types.

Experimentally it was decided that for composite propellants a choice should be made between the conflicting explanations which are based respectively on the chemical nature of the oxidizer or the over-all ballistic properties of the propellant. By an exacting propellant

formulation study, it proved possible to produce two propellants with appropriately matched ballistic properties--one containing ammonium perchlorate and ammonium nitrate responded in an unstable manner to a pressure transient, while the other containing potassium perchlorate and ammonium nitrate was stable.

This critical comparison suggests that combustion processes associated with the burning of ammonium perchlorate are to a large measure responsible for the coupling often observed between acoustic waves and the burning of propellant containing ammonium perchlorate. Further confirmation of this has been obtained in Institute T-burner experiments in which pellets of pressed ammonium perchlorate were found to burn unstably.

The specific conclusions reached in the above-referenced phase of our experimental program stimulated renewed study of both physical and theoretical models of the combustion process. In association with a study of propellant extinction, a theoretical model was developed which could permit heat release in the combustion wave to occur in two zones, one characterized by surface reactions as typified by the ammonium perchlorate decomposition flame or perhaps even by heterogeneous reactions, and the other would be normal gas phase combustion away from the surface. The model shows qualitatively that instability would be expected to result from the inclusion of an oxidizer such as ammonium perchlorate. Similarly the observed pressure-burning rate stability boundary is predicted by the theory.

Experimental studies of double-base propellants at high pressures reveal that combustion is usually stable and various types of instability occur as the burning rate and operating pressure are reduced. Significantly, the generation of a finite amplitude traveling wave only occurs for a slow burning propellant at low pressures when the fizz burning zone is relatively thick and the shock pressure of the wave front appears to be able to promote the release of the necessary sustaining energy.

Further investigation of the role binder chemistry plays in the combustion characteristics of propellants was stimulated by the theoretical model developed. A small but definite effect appears to be attributable

to the binder type in the stability bound of ammonium perchlorate-based propellants.

From the standpoint of the rocket motor designer, our over-all studies in typical rocket motors have shown that the inclusion of ammonium perchlorate in propellants almost invariably aggravates a variety of combustion problems. (This is true both for composite and composite modified double-base propellants.) The stability data obtained are of great value in anticipating problem areas and in suggesting ways of designing out specific types of instability if they should occur in a motor required for operational purposes.

II RESEARCH OBJECTIVES

The ultimate objective of this research is to identify the chemical and physical processes responsible for unstable combustion during the burning of solid propellants in rocket motors. The principal specific goal is the understanding of erosive-velocity-coupled instabilities, primarily through the study of finite-amplitude axial instability.

A second specific goal is to provide comprehensive data for use by rocket design engineers in choosing propellants and associated grain configurations for particular applications.

Previous pages were blank, therefore not filmed.

III EXPERIMENTAL AND THEORETICAL PROGRAM

A. General

In the current studies experiments have been performed to further elucidate the influence of propellant compositional factors on instability with a view toward obtaining data suitable for theoretical interpretation. The studies have been based principally on the pulse triggering of longitudinal mode finite amplitude traveling wave instability;¹ supporting investigations have also been performed in other burners. In particular the studies have sought to further define the pressure-burning rate regimes where instability occurs with ammonium perchlorate (AP) propellants containing different fuels and other additives.

Previous studies have shown that for typical composite propellants the presence of ammonium perchlorate usually endows propellants with incipient instability if the burning rate is less than the deflagration rate of AP. (This is a qualitative generalization which has not been completely rationalized with any of the candidate flame models proposed by various workers.)^{2,3,4}

This observation is most significant, since it suggests that rate-controlling processes occur either in the AP monopropellant flame or a modified monopropellant flame (in the latter the temperature profile which controls heat transfer to the surface is modified by other processes such as the inter-diffusion flame of reactants from the pyrolyzing binder). An alternative explanation might also be sought in critical sub-surface reactions, since under certain conditions solid phase decomposition of AP may compete with vaporization and dissociation of AP. To gain information on critical processes associated with AP combustion, pressed pellets of AP were burned in a T-burner and attempts were made to examine the infrared radiation during periods of stable and oscillatory burning. These experiments were planned to gain an insight into the characteristic relaxation time of the combustion processes.

In a further series of experimental studies we examined the propagation and growth of the wave fronts characteristic of finite amplitude traveling wave axial instability.

B. Test Instrumentation

The programmer shown schematically in Fig. 1 was used for automatic programming of all motor test firings. Considerable improvements were necessary in data acquisition methods to obtain good data on wave travel phenomena. Specifically, techniques were developed to record and play back pressure data from multi-station high frequency pressure transducers which were located along the length of the rocket motors investigated. This improved instrumentation has enabled both amplitude and velocity data to be obtained with sufficient accuracy to identify where critical driving and damping processes occur in a motor.

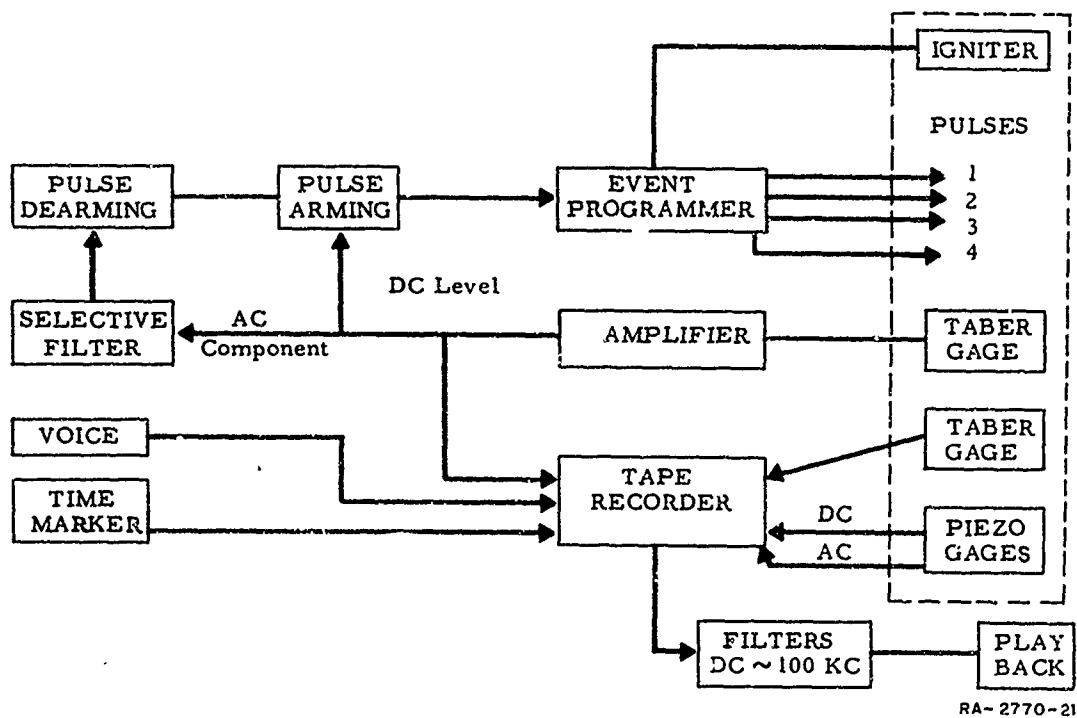


FIG. 1 INSTRUMENTATION BLOCK DIAGRAM

The programmer automatically sequences all events called for in a test firing such as recorder switch-on, camera run-up, igniter light-off, and pulse initiation.

C. Rocket Motor Configuration

Static firings of the various propellants investigated were usually carried out in a 5-inch-diameter chamber whose length could be varied from 7 to 80 inches. The standard 40-inch-long chamber is shown in Fig. 2; a multi-unit pulse head is attached at the head end and a relatively aerodynamically clean closure fitted with a pressure relief device is attached at the aft end.

While tubular grains were normally used in studies on compositional factors, grains with rectangular perforations were necessarily used in the wave propagation studies (Fig. 3). The grains were cast into motors which could be fitted with either high frequency transducers or optical viewing ports at selected stations along the length. The rectangular motor fitted with Plexiglas sides was abandoned early in the study, since it was found that at the necessary low design pressures the enhanced stability from the relatively flexible inert side walls precluded unstable operation.

D. Propellants Investigated

In the studies previously reported⁵ many typical operational AP-based propellants used in modern rocket motors were examined, along with some special propellants containing potassium perchlorate (KP), ammonium nitrate (AN), lithium perchlorate (LP), and nitrocellulose/AP mixtures. The previous results⁵ suggested that AP-containing propellants burning in certain regions of the pressure-burning rate surface were unstable. This study has been extended by comparing AP/AN and KP/AN propellants possessing comparable burning rates in regions found to be unstable for AP propellants.

With the recognition that the driving of the finite amplitude traveling wave instability was associated with the chemical and physical processes occurring in combustion waves, it was also decided to

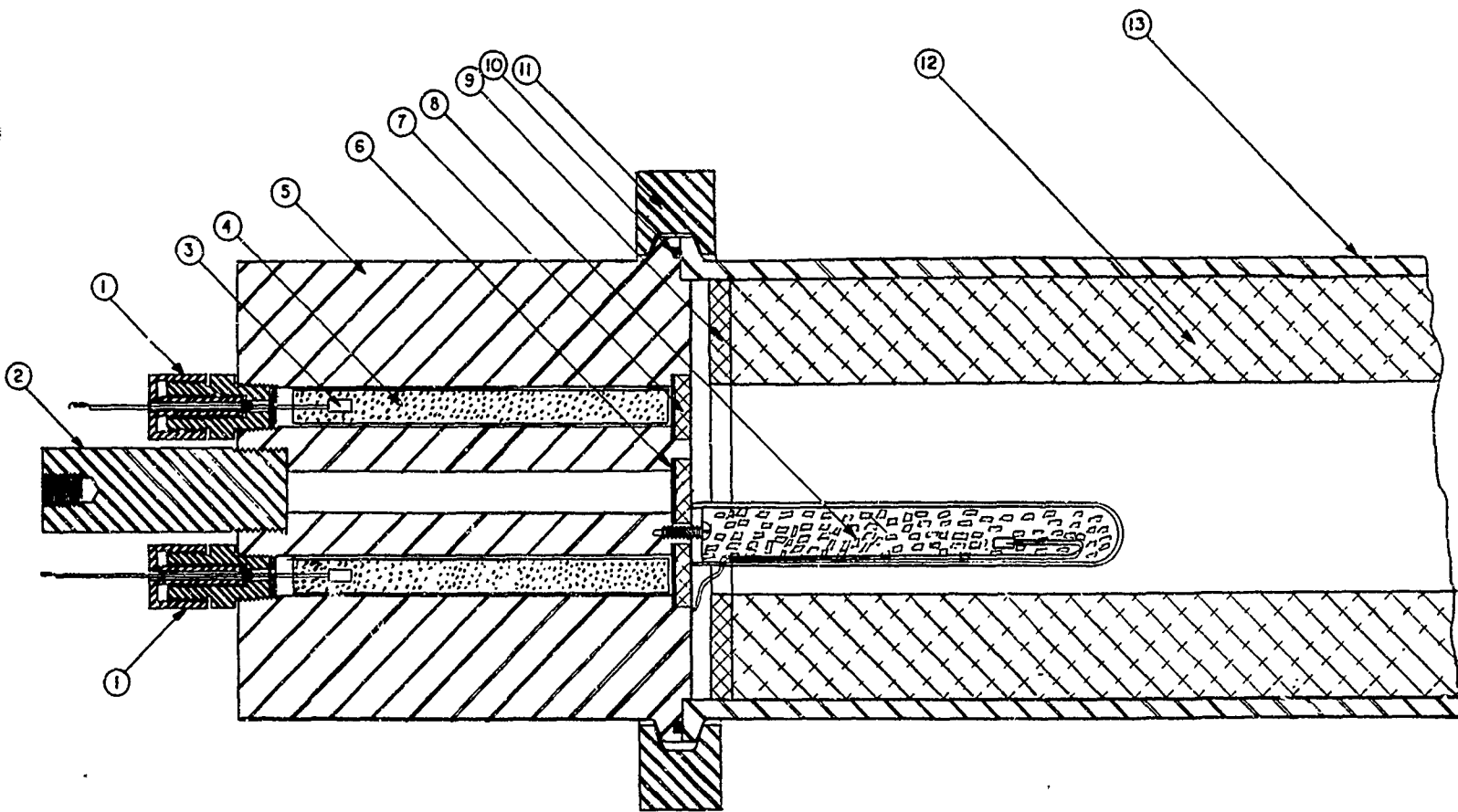
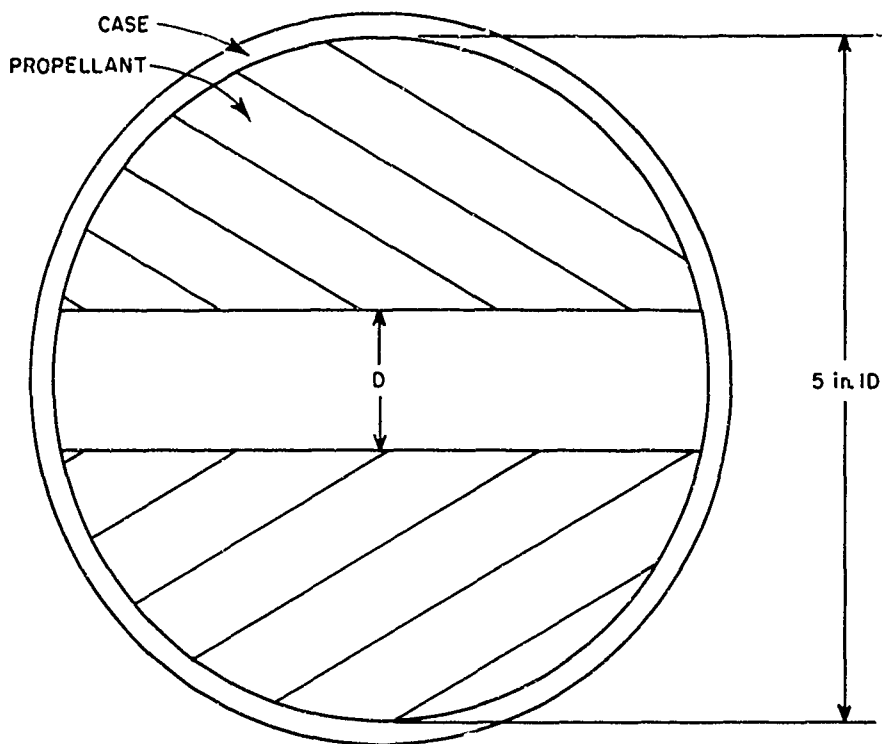


FIG. 2 5-INCH x 40-INCH UNSTABLE COMBUSTION MO

2



D, PERFORATION WIDTH WAS EITHER 1.0 in. OR 0.75 in.

TA-4865-11

FIG. 3 OPPOSED SLAB GRAIN FOR 5-INCH DIAMETER MOTORS

investigate two typical operational double-base propellants. The known differences in the combustion wave would, it was hoped, provide critically needed information on the energy sources responsible for instabilities.

The composite propellants used in this study to date are detailed in Table I, and their nominal ballistic behavior in the pressure range 250 to 2000 psia is outlined in Table II. The double-base compositions investigated are also described in Tables I and II.

Table I
PROPELLANT FORMULATIONS INVESTIGATED

A. Composite Propellants

Propellant Type*	Composition, Percent by Weight				
	APC*	KClO ₄	AN	Binder	Additive
PBAN 102	68.2			16.8	15.0 Al
103	80			20	
104	78.5			20	1.5 LiF
205	75.0			25	
229	79.5			20	0.5 Fe ₂ O ₃
244	79			20	1.0 LiF
284***	79.5			20	0.5 SrCO ₃
PU 125		40	40	20	
127	40		40	20	
146	78.5			20	1.5 Fe ₂ O ₃
PS 115	80			20	

B. Double-Base Propellants

Propellant Type	Description
S	Extruded double base, NC/NG
F	Extruded double base, NC/NG

* PBAN-Polybutadiene acrylic acid acrylonitrile terpolymer;
PU - Polyurethane; PS - Polysulfide

** Bi-model mix; 66% as received, nominal 100 μ, and 34% ground
11 μ.

*** Tri-model mix; 50% as received, 25% 20 μ, and 25% 600 μ.

Table II
PROPELLANT BURNING RATE DATA

Propellant Type	Burning Rate, msec at Pressure psia				
	250	500	1000	1500	2000
PBAN 102	0.185	0.25	0.33	0.38	
102M	0.200	0.270	0.350	0.42	
103	0.165	0.22	0.28	0.30	
103M	0.185	0.255	0.33	0.37	
104	0.14	0.225	0.23	0.24	
205	0.135	0.185	0.23	0.25	
229	0.235	0.315	0.42	0.5	
244	0.135	0.200	0.235	0.27	
284	0.135	0.215	0.230	0.245	
PU 125M	---	0.068	0.136	0.176	
127	---	0.062	0.126	0.163	
146	0.245	0.32	0.375	0.44	
PS 115	0.25	0.34	0.47	0.56	
S	---	0.26	0.37	0.45	0.525
F	---	0.56	0.80	0.95	1.0

E. Theoretical Studies - Combustion Models

The nature of the chemical reactions and associated physical processes controlling the burning rate of ammonium perchlorate-based propellants is still largely a matter of conjecture; consequently any attempt to develop theoretical models appears to be fraught with grave uncertainties. Nevertheless it was decided that an attempt should be made to theoretically reconcile the large volume of experimental data accumulated in this program which relate instability to propellant composition.

A combustion model being developed in another program related to propellant extinction characteristics⁶ has provided the framework for testing whether significant differences noted between ammonium perchlorate

and other oxidizers could be explained on the basis of recognized differences in combustion wave characteristics.

F. Scaling Studies

The determination of amplitude growth of the traveling wave during propagation along the length of a rocket motor permitted, through application of numerical analysis, an attempt to generate scaling laws.

The interdependence of many ballistic design parameters permits only slow progress in this area, but experiments were designed to cover a limited number of motor aspect ratios.

In previous work⁵ an attempt was made to develop a scaling relationship based on similitude studies between wave travel times associated with an instability and critical mixing times which could be predicted on the basis of turbulent mixing processes in a 'granular' diffusion flame. During the current investigation this modeling approach was critically examined by investigating the influence of both changes in wave travel time, by varying motor length, and changes in critical mixing geometry, by varying propellant microstructure.

IV EXPERIMENTAL RESULTS

The experimental studies were designed to elucidate the nature of critical processes within the combustion wave which control the onset of combustion instability. To facilitate this study the roles played by propellant compositional factors and motor geometry were examined in a variety of motor types.

A. Propellant Compositional Influence

1. Composite Propellants--Rocket Motor Studies

The previous program⁵ had shown that the inclusion of ammonium perchlorate in a composite or composite-modified double-base propellant generally increased the incidence of combustion instability (data on instability are summarized in Fig. 4).

In ammonium perchlorate-based propellants a stability bound exists which divides the pressure burning rate surface into two regions; one where any finite amplitude disturbance will decay, and another where it may amplify, forming a traveling wave whose net amplitude is governed by the driving and damping present in the cavity. Contrariwise, no motor operating conditions were found in studies with the 5-inch-diameter by 40-inch-long motor where traveling wave instability could be excited in potassium perchlorate, lithium perchlorate, or ammonium nitrate-based propellants.

The metallic salt oxidizers produce propellants which burn considerably faster than uncatalyzed AP-based propellants; the AN-based propellants burn considerably slower. Catalyzed fast-burning AP propellants were shown in our study to operate completely within the stable regime found for AP-based propellants. In view of these past observations it was considered imperative to resolve whether the macro-ballistic phenomena of burning rate, affecting as it does the thermal relaxation times for the gas and solid phases, was the critical factor or whether the physical and chemical processes associated with AP combustion controlled the incidence of instability.

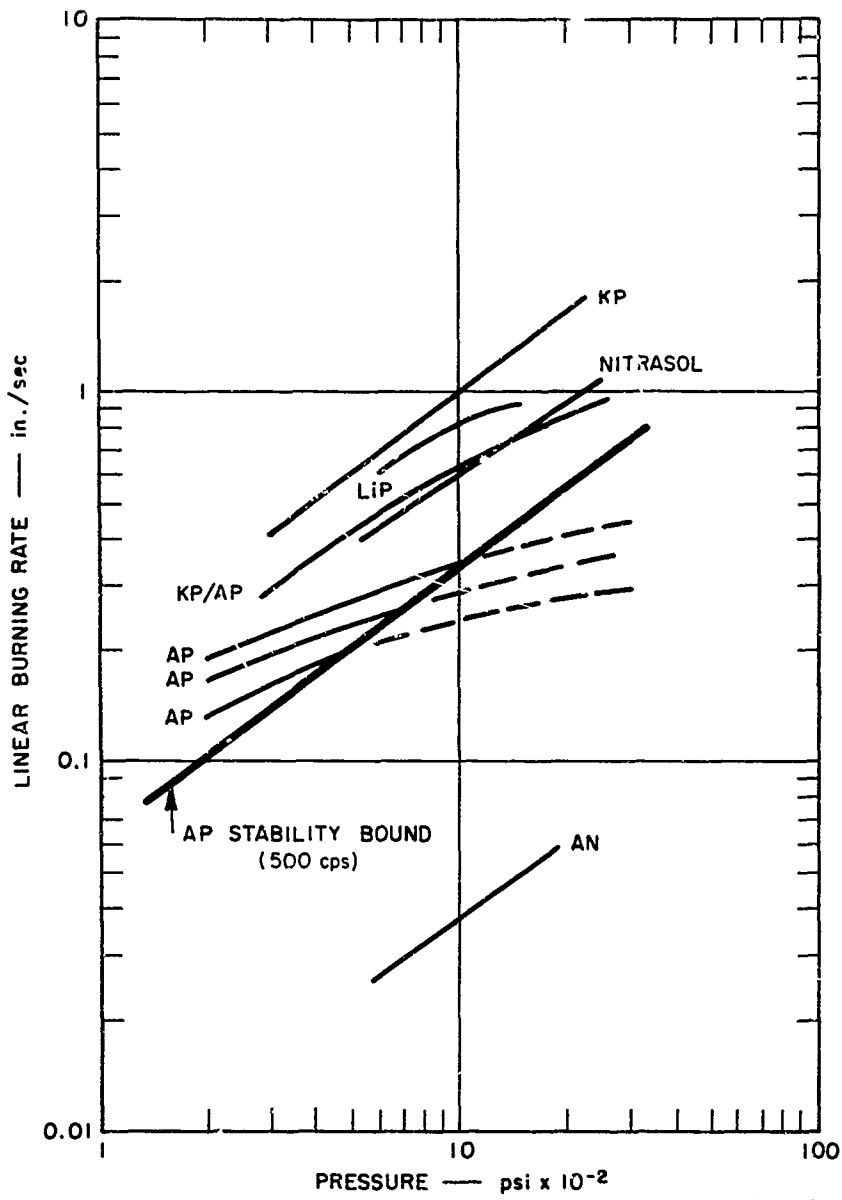


FIG. 4 TYPICAL PROPELLANT BURNING RATE CURVES RELATIVE TO STABILITY BOUND FOUND FOR PROPELLANTS CONTAINING AMMONIUM PERCHLORATE: SOLID LINE, STABLE BURNING REGIME; DOTTED LINE, UNSTABLE BURNING REGIME AS DETERMINED IN A 5-INCH x 40-INCH MOTOR (Data Obtained from Reference 5). Aluminized Nitrasol Propellant Unstable in One Firing.

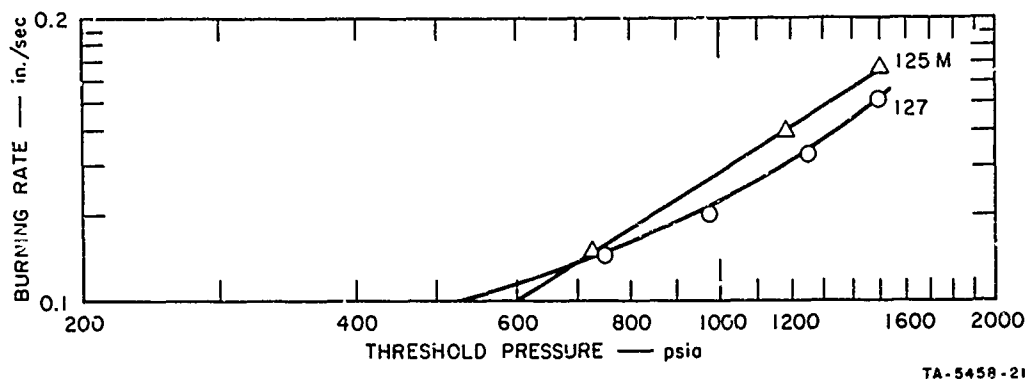


FIG. 5 PROPELLANT BURNING RATE DATA FOR PROPELLANTS PU 125M AND PU 127 (PU 127 Containing AP and AN Burned Unstable While the Other Propellant Containing KP and AN was Stable)

To resolve the issue it was decided to attempt the formulation of two propellants with matched ballistics; one was to contain AP and AN and the other KP and AN. After an extensive, and fortunately successful, propellant formulation study, two propellants were obtained whose burning rate-pressure relationship (Fig. 5) lay in between the AP stability bound and the burning rate relationship for the catalyzed AN propellants previously studied.

The two propellants were initially test-fired in a 5-inch x 40-inch motor with a radial burning grain. It was found that the propellant containing KP and AN (PU 125-M) was quite stable to pulsing; the other propellant, containing AP and AN (PU 127), became unstable and the safety device ruptured. The pressure-time trace of the firing showed a few cycles of the characteristic traveling wave superimposed on a rapidly rising chamber pressure.

In order to examine the response of the propellant it was decided to attempt to follow the wave form of the instability transients in a motor operating at a sufficiently low pressure so that rupture of the safety device would not occur. Difficulties in igniting ammonium nitrate-based propellants as well as the safety advantage of operating with a regressive grain led to the use of the slab propellant grain in the

5-inch motor. The slab motor was pulsed twice and the pressure-time curve shown in Fig. 6a was obtained.

A detailed examination of the high frequency response transducer records (Figs. 6b and c) showed that the amplitude of the traveling wave decreased steadily as the mean chamber pressure rose; eventually the wave disappeared, and the mean chamber pressure decayed to a level lower than the predicted steady state value (Fig. 6b). This experimental result is interpreted on the basis that during the period of instability the ammonium perchlorate oxidizer is burned preferentially; this leads to a depletion of ammonium perchlorate at the surface. The steady state pressure of course depends on burning of both AP and AN; consequently, depletion of AP leads to operation at a reduced pressure until the surface concentrations of each oxidizer return to the mean values existing before the disturbance.

It is considered that this comparison between the AP/AN and KP/AN propellants conclusively proves that instability can be traced to one or more critical processes occurring in the deflagration of AP and its interdiffusion flame with the pyrolyzed binder. To unequivocally demonstrate that the monopropellant flame of AP could sustain instabilities, an examination of AP combustion in a suitable burner was planned.

2. Monopropellant Combustion of AP

As a consequence of our previous investigations⁵ showing, in the case of AP, the strong dependence of the threshold pressure for instability on the burning rate of the propellants, it was considered desirable to examine the over-all response of combustion processes in the decomposition of AP. This work was further prompted by the theoretical studies of Sotter⁷ on the chemical kinetics in the gas phase zone of double-base propellants; he concluded that only a few reactions were sensitive enough to pressure perturbations to contribute largely to the response of double-base propellants. The heterogeneous composite propellant, however, probably presents a more complicated picture. Price⁸ has concluded that the response of the reactions occurring in the diffusion flame are

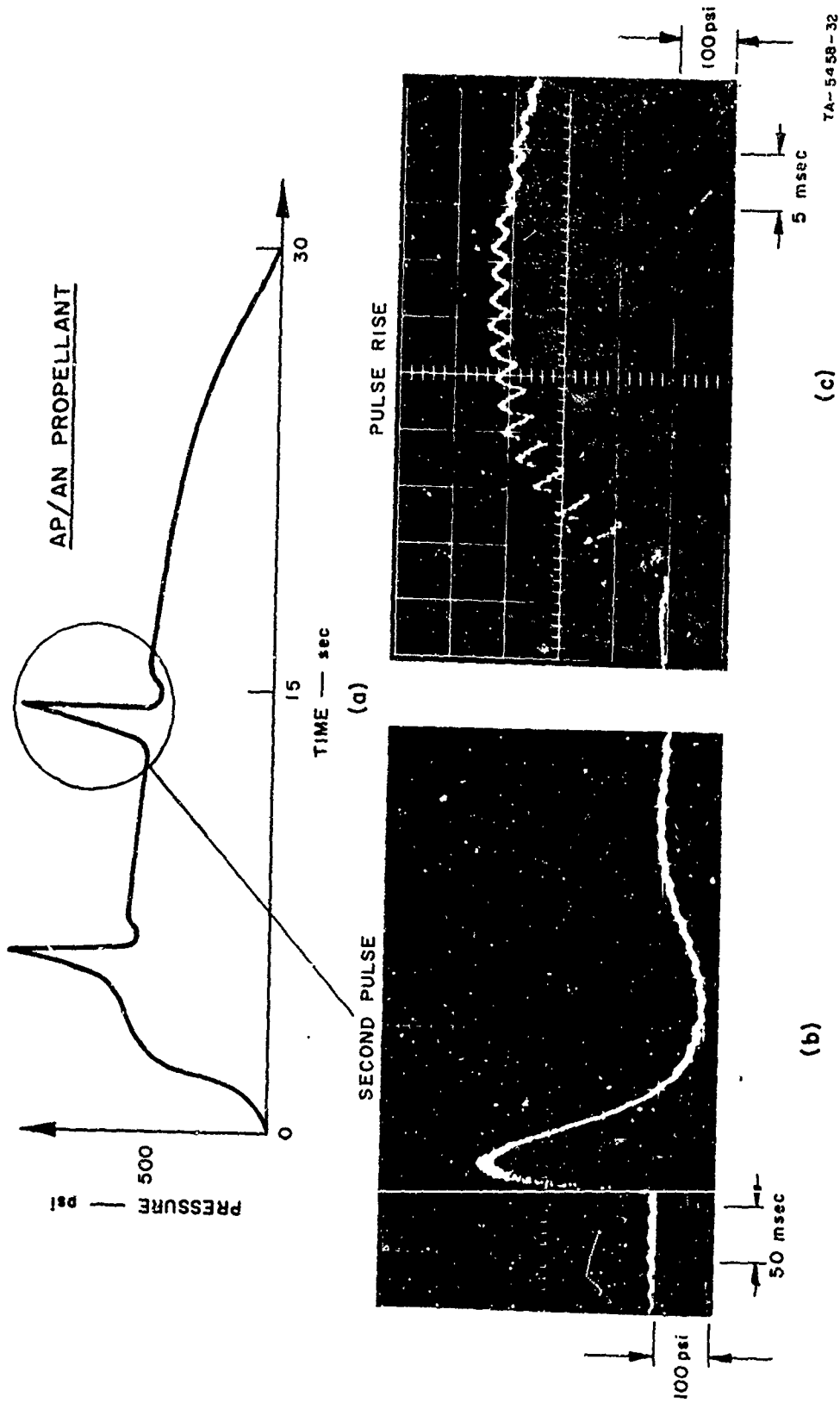


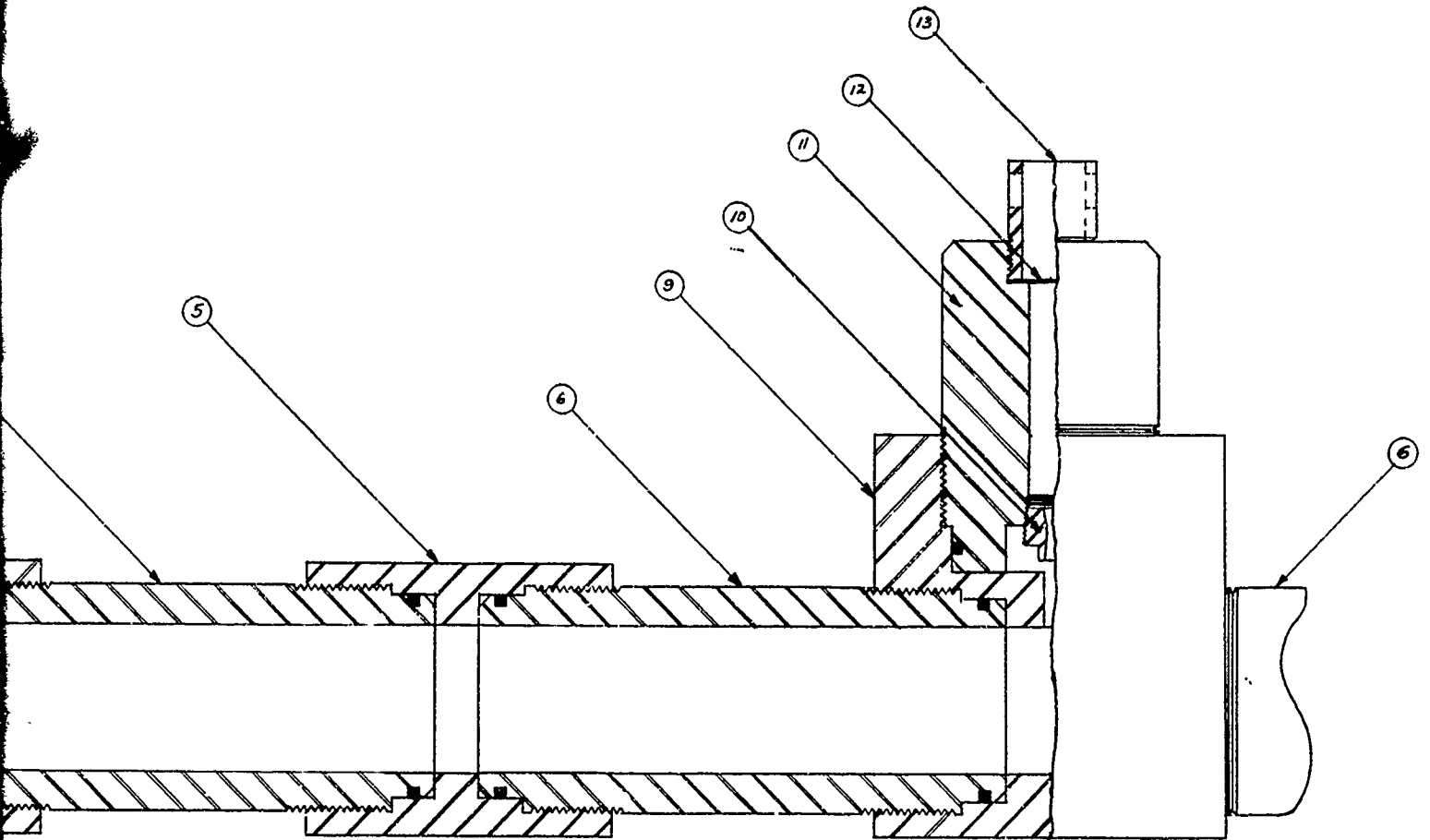
FIG. 6 (a) PERFORMANCE CURVE PRESSURE vs. TIME FOR AP/AN PROPELLANT (PU 127) SHOWING BALLISTIC BEHAVIOR ON PULSING; (b) OSCILLOSCOPE PLAYBACK RECORD OF SECOND PULSE SHOWING OVERALL PRESSURE RESPONSE DURING 300 msec PRESSURE EXCURSION; (c) HIGH RESPONSE OSCILLOSCOPE PLAYBACK SHOWING GROWTH AND DATA OF AXIAL INSTABILITY DURING THE GROWTH OF THE PRESSURE EXCURSION

responsible for the acoustic interactions leading to sustained combustion instability. In our study in the T-burner, the decomposition of the simplest component of the heterogeneous propellant system, ammonium perchlorate, was examined in relation to its contribution to combustion instability.

The response of burning AP to pressure perturbations was studied in a 2-inch-diameter T-burner similar to that described by Price and others.⁹ Ammonium perchlorate pellets $1\frac{1}{2}$ -inches in diameter x $\frac{1}{2}$ -inch thick were pressed at a pressure of 210,000 psia to give a density of 1.94 g/cc. (This is 99.5% theoretical; decrease in density resulted in a lower degree of instability.) The ammonium perchlorate used was of high purity with less than 10 ppm of impurities. The pellets were mounted at each end of the 40-inch-long burner shown in Fig. 7. A specially shaped window was used to view radiation above the surface of the pellet. The pellet was burned at pressures above 400 psia, since this was found to be the minimum deflagration limit for the AP used in our experiments. The burner was consequently pressurized with nitrogen to 400 psia and the increase in pressure after ignition then burst a diaphragm held in place over the nozzle.

In initial experiments the pressure response was monitored with Kistler gages in Type 622B mounts located in the side of the T-burner at the level of the pellet surface. Subsequently the response of emitted infrared radiation at 2.26 and 3.10 microns was monitored by means of a quartz window mounted to view the burning surface. The infrared radiation was detected with the apparatus sketched in Fig. 8.

It was found that burning AP would oscillate in the T-burner at amplitudes varying from 5 to 80 psi at mean chamber pressures in the range 600-800 psi. In the same burner neither potassium perchlorate propellants nor high burning rate AP propellants would oscillate. In Fig. 9 typical oscillations measured by the Kistler gages at each end of the T-burner are shown on oscillograms. It appeared that the unequal amplitudes measured at opposite ends are characteristic of uneven burning over the face of the pellets; i.e. one pellet presented less burning



ITEM	DWG. NUMBER	DESCRIPTION	QTY.
13		DIAPHRAM RETAINER	1
12		BURST DIAPHRAM	1
11	C-542	NOZZLE ADAPTOR	1
10		NOZZLE	1
9	C-541	ADAPTOR BLOCK	1
8		QUARTZ WINDOW	1
7		WINDOW RETAINER	1
6	C-539	SPACER	6
5	C-540	COUPLER	6
4	C-539	SAMPLE HOLDER	2
3		PRESSURE TRANSDUCER	2
2		PROPELLANT SAMPLE	2
1	C-538	END CAP	2

MATERIAL: 1015 STEEL		TOLERANCES:	BASIC DIMS.	FRACT. FOL.	DIMENAL FOL.
PROCESS: MACHINE		DECIMALS	± 1/32 IN.	± 1/16	± .002
DR. [Signature]		ANGULAR FOL.	± 1/2°	± 1/4°	± .002
COP. [Signature]		± 1/2°	± 1/4°	± 1/4°	± .010
TITLE: TEE BURNER ASSEMBLY					
APPV. [Signature]			NEXT ASSEMBLY:		SCALE: FULL
STANFORD RESEARCH INSTITUTE MENLO PARK, CALIF.				DWG. NO. D-564	

R FITTED WITH INFRARED VIEWING PORT AND PRESSURE

FIG. 7

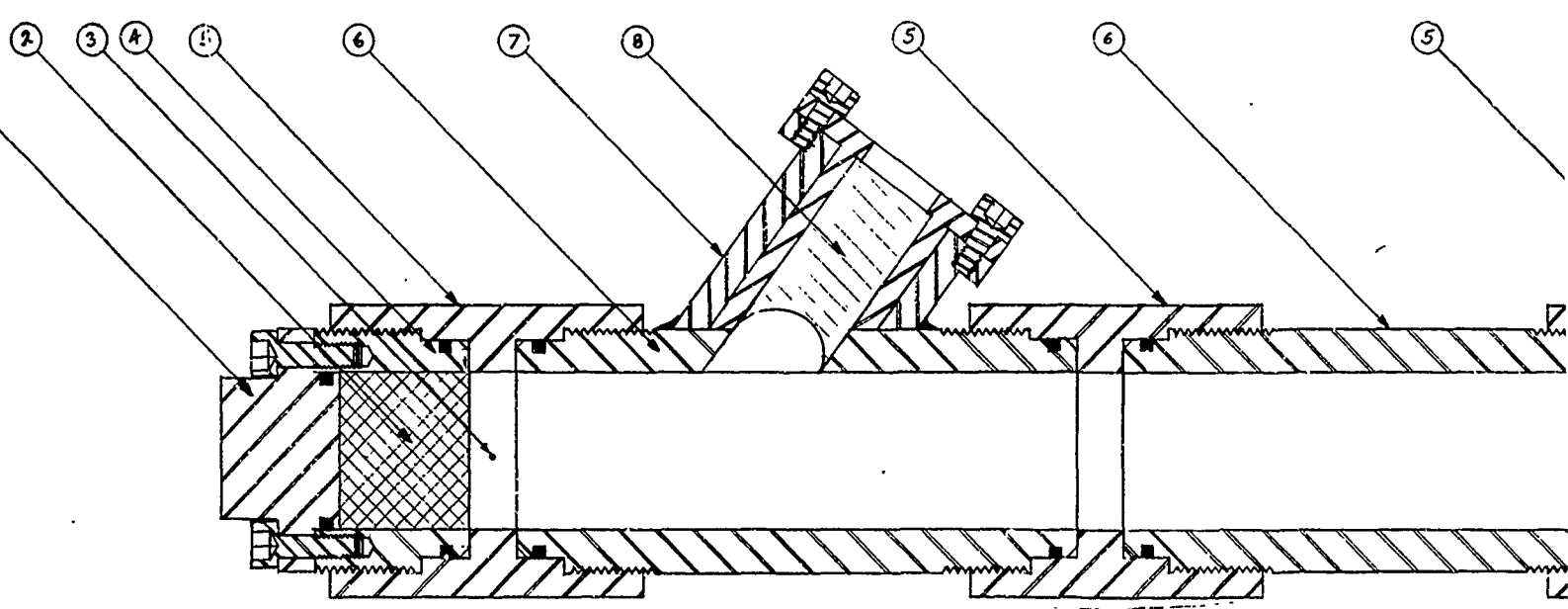


FIG. 7 40-INCH LONG ACOUSTIC BURNER FITTED WITH INFRARED TRANSUCERS

2

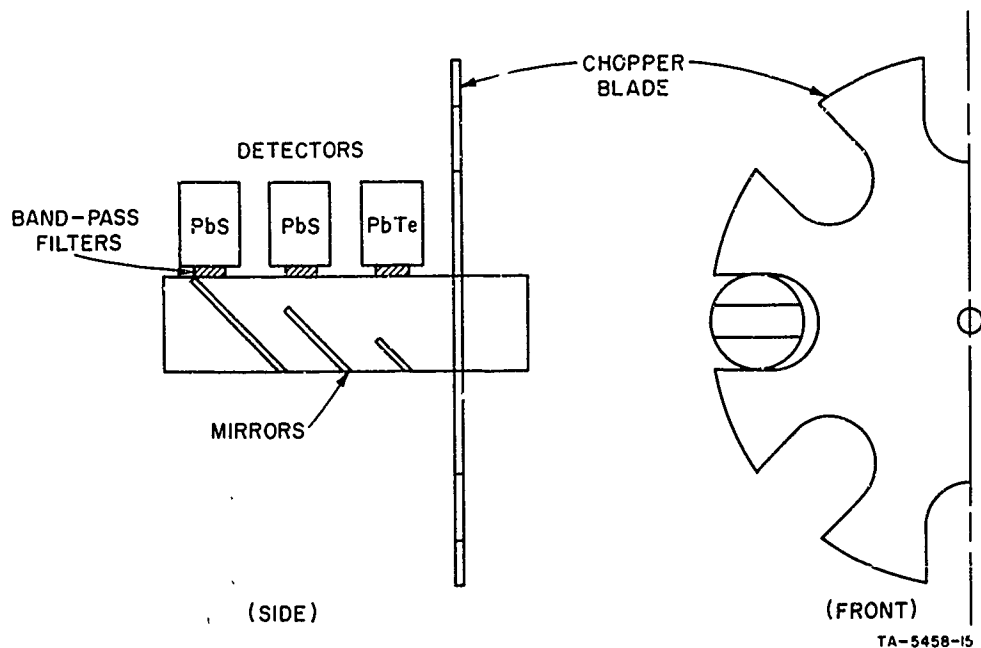
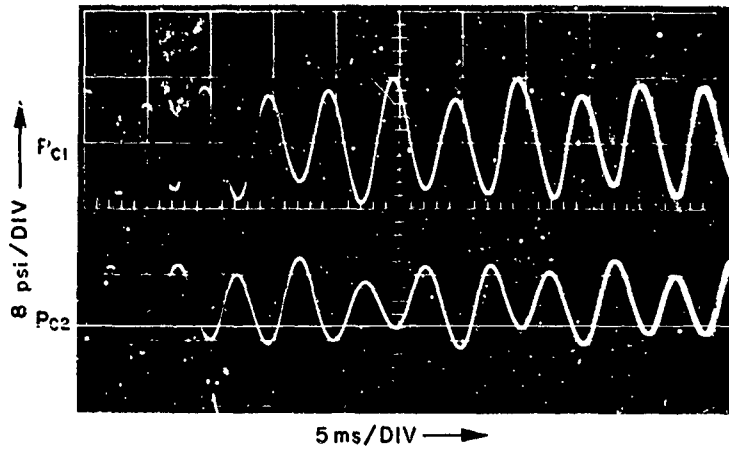


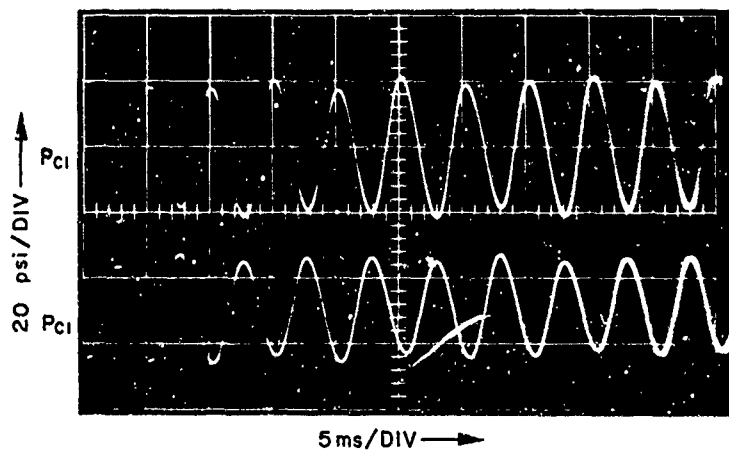
FIG. 8 SCHEMATIC LAYOUT OF INFRARED RADIATION DETECTION DEVICE

surface to couple with the acoustic cavity. The frequency of 200 cps is characteristic of a standing acoustic wave possessing a pressure antinode at the center of the burner.

In Fig. 10a are shown oscillograms of pressure and infrared light measurements made on AP pellets burning unstably in the T-burner; P_{c_1} and P_{c_2} are Kistler gage measurements at the burning surface at opposite ends. $I_{2.26}$ and $I_{3.1}$ are light intensities at 2.26 and 3.1 microns from the AP pellet corresponding to the location of P_{c_1} . In Fig. 10b the over-all pressure-time trace is included along with the D.C. pressure level to show both the absolute pressure level and the occurrence of instability. The burner was pressurized to 400 psig before ignition; pressure then built up until the diaphragm ruptured at 650 psig. The maximum peak-to-peak amplitude observed during unstable operation has varied from 20 to 80 psi. The data gaps shown on the light intensity traces are caused by the light chopper, operating at 20 cycles/sec, which was used to eliminate detector saturation problems.



(a)



TA-5453-16

(b)

FIG. 9 PRESSURE OSCILLATIONS OBSERVED DURING UNSTABLE BURNING OF PRESSED AMMONIUM PERCHLORATE PELLETS

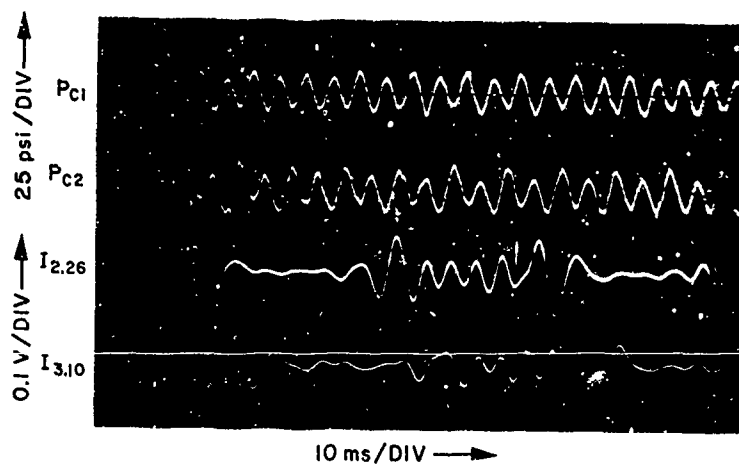
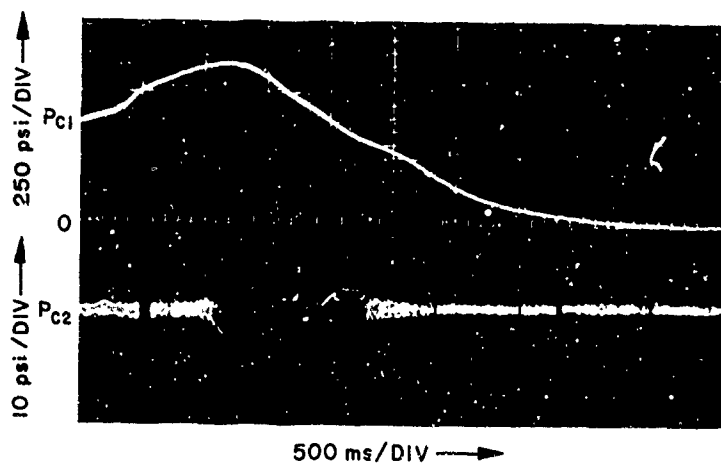


FIG. 10(a) OSCILLATIONS IN PRESSURE AND INFRARED RADIATION OBSERVED DURING THE BURNING OF PRESSED AMMONIUM PERCHLORATE PELLETS (Test 63)

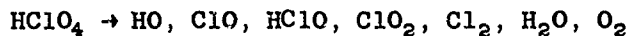
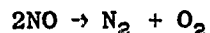
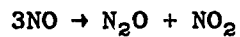
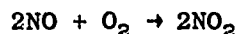
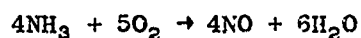


TA-5458-17

FIG. 10(b) PRESSURE/TIME TRACE, D.C. AND A.C. COUPLED, OBTAINED DURING COMBUSTION OF PRESSED AMMONIUM PERCHLORATE PELLETS

In our studies of infrared radiation from deflagrating AP, the two wavelengths of 2.26 μ and 3.1 μ were selected, since a considerable amount of data on the emission and transmission characteristics of these wavelengths had been accumulated by Powling and Smith.^{10,11} At the high pressure used and in our experiment the detectors monitored the temperature response of the gases above the surface of the AP. It is concluded that our measurements at 2.26 and 3.1 μ represent the temperature response of the gas phase above the burning surface. It will be noted in Fig. 10a that the temperature perturbation (as measured by response of the lead sulfide cells at the specified wavelengths) is out of phase with the pressure perturbation. The exact meaning of this is not clear at this time. Preliminary experiments using AP propellants rather than pressed pellets show that the phase relationship between light radiation and pressure is also a function of the light detector location above the burning surface and the absolute pressure level of the test chamber. It may also be dependent upon the apparatus geometry. It is therefore not possible to attribute any phase lags, or leads, between pressure and light radiation at this time to thermal relaxation times in the solid or gas phases, nor to departures from equilibrium.

The experimentally observed sensitivity of AP pellets burning in the T-burner to acoustic pressure perturbations could perhaps be satisfactorily explained on the basis of the pressure and temperature sensitivity of reactions such as:



which have been identified as possible decomposition reactions.¹² The introduction of a secondary hydrocarbon fuel with the concomitant problems such as additional competitive reactions and the fluid dynamic processes of diffusion and turbulent mixing would further complicate the picture.

In summary, it is apparent that the decomposition of pure AP pellets tends to couple with the acoustic cavity of a T-burner and burn unstably. In analytical approaches it has been customary to neglect this and the response of gas phase reaction, since the times involved were insignificant relative to the frequencies under consideration in this study. It is hoped in future work to elucidate the exact nature of the relaxation phenomena involved and satisfactorily include them in an analytical model.

3. Double-Base Propellants--Rocket Motor Studies

Recognizing that the structure of the combustion wave of double-base propellants is quite different in character from that of composite propellants, it was decided to examine two extruded double-base compositions in addition to the nitrasol propellant previously examined.⁵

It will be recalled that the composite modified double-base propellant previously studied was a relatively fast-burning propellant; in view of this, a fast-burning and a slow-burning extruded double-base composition were selected. These propellants were made available to this program by courtesy of the Naval Ordnance Test Station and the Naval Propellant Plant. The grains obtained were a nominal 5 inches in diameter and possessed a star center perforation; while this was a departure from the simple radial burning grains previously used, this change was not, on the basis of past experience,¹³ considered an important factor in the assessment of axial instability test data. This change in grain design, however, resulted in a more neutral pressure-time curve, and several firings were needed to cover the pressure range of interest.

The experimental test data showed that the fast-burning (F) propellant grains were stable to axial pulsing in the range 650-2200 psia; lower pressures could not be studied because of the adverse effect of motor hardware design on the ballistic design parameters. Incipient transverse instability was observed with this propellant in the pressure range 650-1750 psia.

The slower-burning propellant (S) was found to respond unstably to axial pulsing at 650 psia; at a higher pressure of 2100 psia the propellant

was stable. The stability regimes for transverse instability appeared to follow the same pattern in that no high frequency instability was detected at elevated pressure.

The instability trends observed with the extruded double-base propellants are shown in Fig. 11. It is considered that the occurrence of axial instability at low pressures with low burning rate propellants can be explained on the basis of the increase in fizz burning reaction zone thickness as the pressure is lowered. Increase in pressure increases the over-all reaction rates in the gas phase and consequently gas-flow perturbations do not lead to the local instantaneous increases in energy release necessary to sustain a traveling wave type of instability.

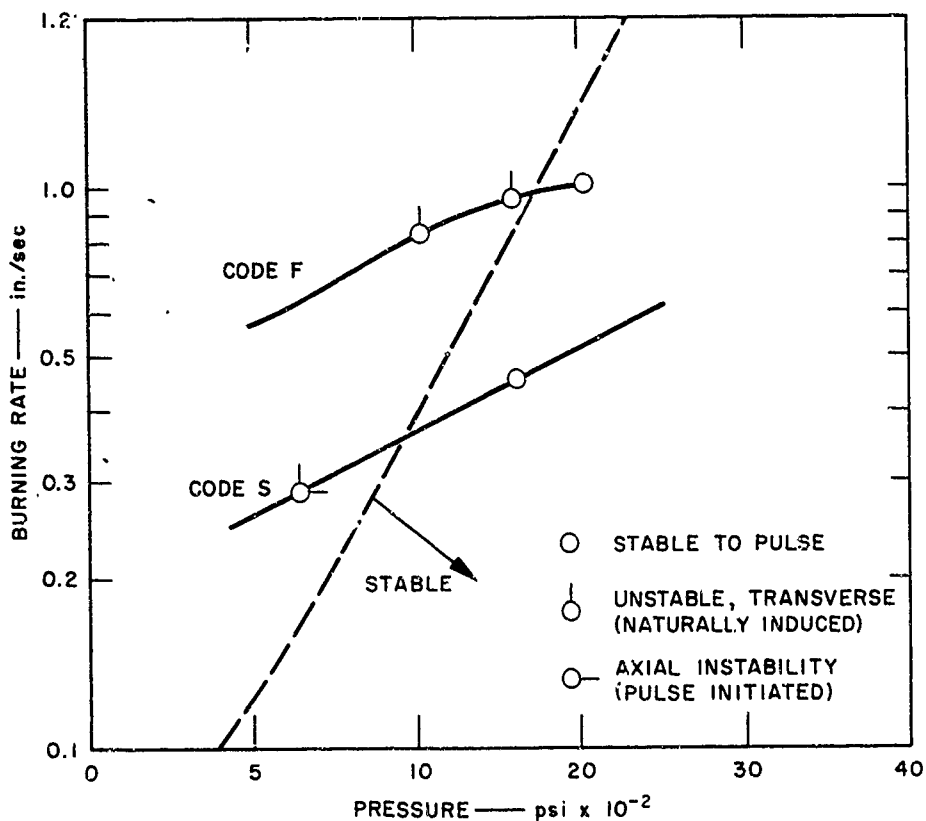


FIG. 11 SUMMARY OF INSTABILITY DATA FOR TWO REPRESENTATIVE DOUBLE-BASE PROPELLANTS, SHOWING STABLE OPERATION AT ELEVATED PRESSURES; STABILITY BOUND IS SUBJECT TO FURTHER EXPERIMENTAL CHARACTERIZATION

B. Combustion Models

1. Theoretical Studies

Most theoretical investigations of combustion instability in solid rockets have emphasized the role of gas dynamics in the combustion chamber, paying less attention to the combustion mechanism of the propellant itself. It has become customary to describe the behavior of the latter in terms of an essentially empirical factor, the "acoustic admittance." In view of the enormous complexity of the solid propellant combustion mechanism, which is not well understood even in steady-state operation, this is a reasonable approach and it has proven useful. However, something more than an empirical representation of the propellant's combustion mechanism certainly is a prerequisite for a comprehensive understanding of transient phenomena in solid rockets. Accordingly, theoretical studies conducted during this program have been concerned primarily with the propellant response.

Our objectives in these studies extend somewhat beyond the specific problem of combustion instability, for one can anticipate that the controlling mechanisms during instability phenomena will be of comparable significance in any combustion transient having a similar characteristic time. For example, it has been our expectation that a valid model of transient combustion would be applicable not only to this combustion instability investigation, but also to combustion extinguishment studies now underway at the Institute. The preliminary results presented in this report appear to confirm this viewpoint. Indeed, to some degree the various transport phenomena are inseparable or very closely related, from the standpoint of the response of the combustion mechanism. Therefore, it is appropriate to begin the theoretical discussion by briefly considering the current quasi-steady analyses of combustion extinguishment, which represent the most recent theoretical approach by others relevant to the transient response of a burning solid propellant. A brief review of these analyses permits a clearer and more complete explanation of the theoretical studies performed during this program, and it provides the background for an interpretation of the theoretical relationship between

combustion instability and extinguishment criteria which is derived in the present work.

2. Assumptions and Limitations of Quasi-Steady Analyses of Combustion Extinguishment

Von Elbe¹⁴ and Paul¹⁵ have independently developed essentially identical analyses of the response of a burning solid propellant to a pressure transient. These analyses incorporate the following assumptions:

1. The rate of change of heat flux (or pressure) is considered to be low enough that there is no appreciable lag in the relaxation of the temperature profile in the grain. Thus there is always a steady state profile corresponding to the instantaneous heat flux.

2. The steady-state burning rate of the propellant is assumed to be described by the empirical expression $r = bP^n$ (see section on Nomenclature for definition of symbols). In addition, this expression is assumed to relate the instantaneous burning rate and pressure during transients.

3. The surface temperature is assumed to be constant.

These assumptions permit a quasi-steady treatment of the response of the propellant to pressure transients. In this approach the empirical steady-state burning-rate law is combined with an energy balance at the gas-solid interface, and the resulting equation is differentiated with time to relate instantaneous burning rate to pressure decay rate.

The limitations of the quasi-steady approach can be deduced by examining the characteristic relaxation times associated with the gas-phase and solid-phase processes involved in the combustion mechanism. Orders of magnitude of these relaxation times are⁶

$$\tau_{\text{solid}} \sim \frac{K_s}{r^2}$$

$$\tau_{\text{gas}} \sim \frac{K_g}{r^2}$$

where K_s and K_g are the thermal diffusivities of the solid and gas phases, respectively. A typical value for K_s is 2.5×10^{-4} in.²/sec, so for a burning rate of 0.1 in./sec the thermal relaxation time in the solid is of the order of 0.025 sec; for a burning rate of 0.5 in./sec it is about 0.001 sec. The gas-phase thermal diffusivity K_g is about an order of magnitude smaller than K_s , with a corresponding reduction in gas-phase relaxation times. Consequently, the solid-phase thermal lag should be the rate-limiting mechanism in extinguishment of burning solid propellants, as assumed by the analyses mentioned above, if unanticipated slower mechanisms do not appear during the transient period. However, this conclusion also implies that characteristic times for extinguishment will be comparable to the solid-phase relaxation time, and, indeed, the extinguishment times observed by Paul et al¹⁵ are in the range 0.005-0.040 sec, or about the same as the relaxation times quoted above. Under these circumstances the quasi-steady analytical approach to the problem is somewhat questionable; such an approach is truly valid only when all relaxation times are negligible relative to the characteristic time of the process under consideration.

The empirical steady state burning-rate law $r = bP^n$ describes a behavior that results from an enormously complex interaction of gas-phase and solid-phase processes. For example, the over-all pressure sensitivity, represented by the exponent n , encompasses the individual pressure sensitivities of many reactions, both in the gas phase and at the interface, and is determined by the order of these reactions and other factors. Inasmuch as the relaxation times of gas-phase and solid-phase processes differ by an order of magnitude, it is likely that the relative contributions of these portions of the burning mechanism to the over-all pressure sensitivity are substantially altered during transient operation. This means that the pressure exponent n may itself be a function of dP/dt , in which case a representation of the burning rate during transient periods by the steady-state expression $r = bP^n$ would be misleading.

It is undoubtedly true that the surface temperature of a burning solid propellant is nearly constant, even with wide excursions in the

burning rate. This observation merely reflects the fact that the effective activation energy E for the surface volatilization process is generally quite large, so that $E/RT_w \sim 10$ or greater. Therefore, purely from the standpoint of determining a temperature profile, the surface temperature can be considered constant. On the other hand, to be self-consistent an analysis to determine the transient behavior of the burning rate may be required to account for changes in the surface temperature, because large changes in the burning rate actually are inseparably coupled through the burning mechanism to small, but finite surface temperature variations.

Because all relaxation times are neglected in the quasi-steady analyses of propellant extinguishment, these theories predict an instantaneous response of the burning rate to an imposed pressure gradient. This implies that at the very instant a sufficient pressure gradient has been introduced, before the pressure itself has responded, burning will cease. In practice, of course, a finite decay rate (with a time constant on the order of 5-40 msec, as noted above) is observed. To account for this lag, Paul et al. have introduced an arbitrary, empirical lag factor in their quasi-steady analysis.¹⁵ This device allows a reasonable correlation of data, but is of somewhat limited value, in that the empirical constants in the lag factor vary with experimental conditions; i.e., the lag factor is not universally applicable.

The relaxation phenomena represented by this lag factor are active, of course, in any transient combustion process. In particular, they play a key role in combustion instability, for the latter occurs when the phasing between various steps in the combustion process is such that the reactions reinforce each other and are in resonance with oscillations in the chamber. Under these circumstances there will be a positive feedback of energy into the chamber oscillatory modes, causing unstable operation unless the damping factor in the chamber is very high.

In recognition of the points discussed above, as part of the present program we have initiated an attempt to develop a more comprehensive and fundamental model of solid propellant combustion under transient conditions, with the specific objective of clarifying and relating the mechanisms of

combustion instability, propellant-flame extinguishment, and other transient phenomena. This approach reflects the hypothesis that the same basic mechanisms appear in all transient responses of similar time scales, and that one of the most important links between these transient phenomena is the relaxation time lag described in the preceding discussion. The philosophy underlying this analysis is that the mathematical complexity should be consistent with the available pertinent information, such as data describing the kinetics of the reactions. Therefore, rather than performing an exhaustive analysis of a model that is highly restricted in deference to insurmountable mathematical complexities, we are seeking a more neutral balance between a realistic model and mathematical tractability. Specifically, the model should encompass in a fundamental way, rather than through purely empirical relationships, the recognized basic features of the combustion mechanism, with modifications or improvements dictated by experiments. At the same time, it is consistent with current quantitative knowledge of the combustion kinetics, and with the desirability of minimizing mathematical problems, to describe the reaction steps in highly simplified terms, e.g., by elementary Arrhenius kinetics.

Marxman has reported a preliminary analysis developed with the above requirements in mind.⁶ This theoretical treatment appears as Appendix A in the present report. The chief conclusions, including the theoretical relationship between stability and extinguishment criteria, are summarized below. In a subsequent section the stability criterion, which appears in the analysis in terms of thermochemical parameters of the propellant (activation energies, thermal diffusivity, enthalpies of reaction) is rephrased, in an approximate manner, in terms of the chamber pressure and burning rate. Since these are experimentally accessible variables, a comparison with laboratory measurements obtained during the program is feasible. The theoretical criterion is consistent with the data and offers a possible explanation for the observations.

3. Response of Sinusoidal Pressure Oscillations or an Exponential Pressure Decay; A Stability Criterion

An oscillatory perturbation in the chamber pressure can be expressed as:

$$\tilde{P} = \epsilon \sin \omega t \quad (1)$$

where the ratio of the oscillation amplitude to the steady state pressure is $\epsilon \ll 1$. The corresponding burning rate response derived in Appendix A, assuming $\tilde{r} = 0$ at $t = 0$, is:

$$r = \frac{C_2}{C_P^2 + \omega^2} \left[\omega \exp^{C_1 t} - C_1 \sin \omega t - \omega \cos \omega t \right] \quad (2)$$

where

$$C_1 = \frac{\bar{r}^2}{K} \left[\theta_H \left(\frac{E_H}{RT_w} - m \right) + \theta_D \frac{E_D}{RT_w} - \frac{C_P}{C_S} \frac{\bar{T}_f}{\bar{T}_w} \left(\frac{E/RT_w}{\frac{n+2}{2} + \frac{E_f}{2RT_f}} \right) + \frac{K}{\bar{T}_w \bar{r}^2} \left(\frac{2E}{RT_w} - 1 \right) \left(\frac{\partial \bar{T}}{\partial t} \right)_w \right] \quad (3)$$

$$C_2 = \frac{\bar{r}^2}{K} \frac{E}{RT_w} \left[\theta_H^m + \frac{n}{2} \frac{C_P}{C_S} \frac{\bar{T}_f}{\bar{T}_w} \left(\frac{1}{\frac{n+2}{2} + \frac{E_f}{2RT_f}} \right) \right] \quad (4)$$

Note that

$$\theta_H = \frac{H_H}{C_S \bar{T}_w} \exp(-E_H/RT_w) \left(\frac{\bar{P}}{\bar{r}_w} \right)^m; \quad \theta_D = \frac{H_D}{C_S \bar{T}_w} \exp(-E_D/RT_w).$$

Equation 2 indicates a very important stability criterion; if $C_1 > 0$ for a given propellant, imposed pressure oscillations may induce in that propellant an unbounded increase in burning rate with time; i.e., unstable combustion. Because instability-damping mechanisms present in an actual rocket chamber are excluded from the present model, it is not necessarily true that combustion instability must occur when $C_1 > 0$. However, the analysis indicates that combustion instability is impossible only if $C_1 < 0$.

The chamber-pressure decay introduced within the port of a solid rocket to terminate combustion typically has the form:

$$\tilde{P} = \exp^{-\beta t} - 1 \quad (5)$$

(Note that at $t = 0$, $d\tilde{P}/dt = -\beta$ or $dP/dt = -\beta\bar{P}$.) The approximate initial response of the burning rate to this pressure decay is:

$$\tilde{r} = \frac{C_2}{\beta + C_1} (\exp^{C_1 t} - \exp^{-\beta t}) + \frac{C_2}{C_1} (1 - \exp^{C_1 t}) \quad (6)$$

As in the case of a sinusoidal pressure oscillation, unstable combustion may occur when a sudden negative pressure gradient is imposed, unless $C_1 < 0$. In fact, this stability criterion holds quite generally, independent of the type of pressure disturbance that is introduced. Such a criterion is not derivable from the quasi-steady analyses discussed previously.

The physical meaning of the stability criterion can be explained qualitatively by examining the separate terms in Eq. (3). For stable burning it is required that the sum of the negative terms be greater in magnitude than the sum of the positive terms. An increase in the magnitude of the negative terms occurs primarily through an increase in the gas-phase flame temperature, which corresponds to an elevation of the energy release in the gas phase. (The other negative term is practically the same for all propellants.) A high energy release associated with the solid phase, e.g. from exothermic decomposition reactions, contributes to the positive terms and thereby promotes combustion instability. Consequently, for stable burning it is required that the heat release from solid-phase coupled reactions remain less than a certain fraction of the total heat release in the combustion process. Highly exothermic solid-phase reactions are likely to exceed the permissible limit and cause unstable combustion. Moreover, owing to the positive $(d\bar{T}/dt)_w$ term, combustion instability may occur in an otherwise stable motor if there is a pressure disturbance while the steady state temperature profile is still being established within the grain, e.g. just after ignition.

4. Pressure Decay Gradient and Combustion Termination

Obviously, termination of the combustion process will ultimately occur if the pressure excursion results in the chamber pressure falling to zero, regardless of the pressure gradient initially introduced. However, the rate at which the extinction occurs, i.e., the time required for the burning rate to drop to zero, is intimately coupled to the transient response of the combustion mechanism and therefore to the pressure gradient. In practice, for solid-propellant combustion to terminate, it is necessary that the minimum possible lag in the response of the burning rate to a chamber pressure decay be achieved. In an actual motor the chamber pressure initially drops, then rises again as a result of the finite chamber volume and nozzle throat area. If the response of the combustion mechanism is slow, reignition may occur as the pressure starts to rise. It is a consequence of this lag effect that an empirical lag factor, which is not universally applicable, is unavoidable when the quasi-steady theory is used.¹⁵ This difficulty is removed with the present approach, because the finite response time of the combustion mechanism is considered.

A criterion for minimizing the propellant response lag time when under the influence of a pressure decay is obtained by examining the second derivative of Eq. (6). The more negative this derivative, which may be identified as r'' , the faster the burning-rate derivative becomes more negative with increasing time. This characteristic is illustrated schematically in Fig. 12, which shows burning rate vs. time, after a pressure decay is imposed, for three cases: $\tilde{r}' > 0$, $\tilde{r}' = 0$, and $\tilde{r}' < 0$. It is clear that propellant extinguishment will be enhanced by making \tilde{r}'' as negative as possible.

The second derivative of Eq. (6) is:

$$\frac{d^2\tilde{r}}{dt^2} \equiv \tilde{r}'' = \frac{C_2}{C_1 + \beta} (C_1^2 \exp^{C_1 t} - \beta^2 \exp^{-\beta t}) - C_2 C_1 \exp^{C_1 t} \quad (7)$$

Note that the second term on the right-hand side is always negative, as desired, but the first term can be either positive or negative. Specifically, at $t = 0$ the first term is negative only if $\beta^2 > C_1^2$. Thus, the

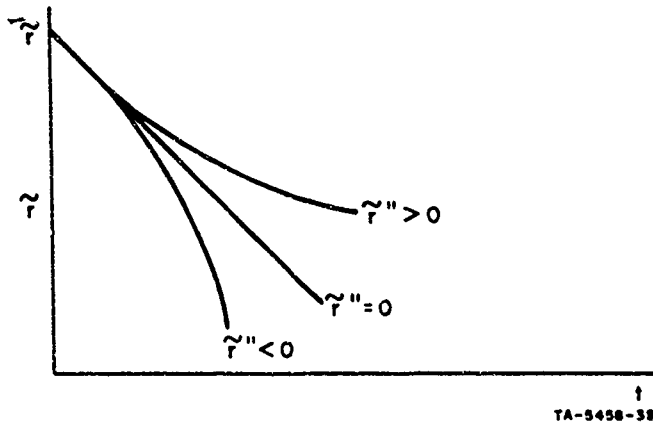


FIG. 12 TIME DEPENDENCE OF BURNING RATE DERIVATIVES

maximum negativity in \ddot{r} , and therefore the most favorable conditions for combustion extinguishment, is achieved if $\beta > |C_1|$.

In summary, the present analysis defines two criteria for extinction of solid propellant combustion: (1) to prevent unstable combustion as a result of pressure disturbances, it is required that $C_1 < 0$; (2) to ensure minimum lag in the burning-rate response of the combustion mechanism to an imposed negative pressure pulse, it is required that $\beta > |C_1|$.

The earlier, quasi-steady analyses of other investigators^{14,15} lead to the following criterion for combustion termination by a negative pressure gradient:

$$\left| \frac{dP}{dt} \right|_{t=0} > \frac{\bar{r}^2}{K} \frac{\bar{P}}{n} \quad (8)$$

where

$$r = b\bar{P}^n$$

The criterion developed in the present treatment, $\beta > |C_1|$, can be expressed in the following comparable form:

$$\left| \frac{dP}{dt} \right|_{t=0} > C_1 \bar{P}, \text{ or} \quad (9)$$

$$\left| \frac{dP}{dt} \right|_{t=0} > \frac{\bar{r}^2}{K} |\lambda| \bar{P}$$

where

$$\lambda = \theta_H \left(\frac{E_H}{RT_w} - m \right) + \theta_D \frac{E_D}{RT_w} + \frac{K}{r^2} \left(\frac{E}{RT_w} - 1 \right) \frac{1}{T_w} \left(\frac{\partial T}{\partial t} \right)_w - \frac{C_p}{s} \frac{T_f}{T_w} \frac{E/RT_w}{\Sigma} \quad (10)$$

The common feature of these two criteria is evident: both show precisely the same dependence on the burning rate, chamber pressure, and thermal diffusivity of the solid propellant. However, the present treatment reveals a basic distinction between different propellants that is not indicated by the quasi-steady analysis. According to Eq. (9), an array of propellants with identical burning rate characteristics, and operating at the same chamber pressure, might still require substantially different pressure gradients to terminate burning, owing to different values of the parameter λ . The magnitude of λ is determined by the relative importance of various reaction phases to the over-all combustion process, while the stability criterion developed above requires that $\lambda < 0$ for stable combustion. Note that those (relatively few) propellants with $C_1 < 0$ will always burn stably in any motor configuration, but in the case of extinction they may require different pressure-decay ratios, inasmuch as these ratios depend upon the magnitude of C_1 . Probably most propellants have $C_1 > 0$, i.e., they can be unstable under certain circumstances. According to Eq. (5) the greater the tendency of such propellants to be unstable (i.e., the greater the magnitude of C_1), the greater the pressure gradient required to achieve the most favorable burning rate response for extinguishment. This theoretical conclusion appears to be in general agreement with experimental observations by Stanford Research Institute investigators^{5,6} and others.

For the first time this analysis establishes a direct, physically realistic, link between instability and extinguishment criteria, showing that the latter depends upon the former. It also affords a possible

explanation for the observed differences in stability characteristics among propellants. As with extinguishment behavior, two propellants with identical burning rate characteristics and equal over-all energy release per unit mass, operating under the same conditions, may have quite different stability characteristics if the formulations are such that the thermal energy release profile of one is markedly different from the other. It should be noted that the stability criterion applies both to acoustic and finite pressure disturbances.

It is important to recognize that Eq. (9) does not constitute a strictly necessary condition for extinguishment. Any negative pressure gradient, if it can be sustained long enough, will ultimately terminate the combustion process. Consequently, a true extinguishment criterion (i.e., a necessary and sufficient condition for extinguishment) must encompass the internal gasdynamics of the combustion chamber as well as the propellant response, because the pressure-time curve depends on both factors. However, according to the present analysis the most favorable initial propellant response to an imposed pressure decay, from the standpoint of extinguishment, will be achieved when the criterion of Eq. (9) is satisfied.

This analysis must be regarded as preliminary in nature. A more exact mathematical treatment of the same model, which avoids certain assumptions about the temperature profile in the solid phase (Eq. 13, Appendix A), yields a more complicated stability criterion, although the qualitative conclusions are substantially unaltered. Also, comparisons with existing and new data are likely to suggest modifications in the treatment. However, even the present approximate analysis seems quite consistent with experimental studies performed during this program, as will become more clear in the following section.

C. Theoretical Relation of Stability Criterion to Motor Pressure and Propellant Linear Burning Rate

The stability criterion $C_1 < 0$ (or equivalently, $\lambda < 0$) appears in the analysis as a limiting relationship between thermochemical parameters of the propellant. This permits a relatively straightforward physical interpretation, as presented above, but a direct comparison with experimental results is difficult, because in most cases the key thermochemical parameters can be neither measured nor calculated accurately. This situation is typical of all combustion theories in which the reaction kinetics play a dominant role (as opposed to aerodynamically controlled combustion processes). Clearly, the theory cannot be expected to yield a complete, quantitative description of the process, even if qualitatively valid, unless the chief parameters can be determined quantitatively. However, the theory provides an extremely useful means of correlating data and guiding experimental studies, if, through suitable approximations, it can be recast in terms of readily measurable quantities.

The easiest and most common method of characterizing solid propellants is through the burning rate-chamber pressure relationship, which can be determined experimentally relatively easily and with good accuracy. Consequently, it is of considerable value to restate the stability criterion derived in the foregoing analysis in terms of chamber pressure and burning rate, at least in an approximate way. By thus showing the form this criterion should take on an r vs. P plot, it is possible to make a comparison with known stability characteristics of propellants.

To do this we note that Eqs. (15) and (16) in Appendix A can be solved simultaneously to yield:

$$\frac{\bar{T}_f}{\bar{T}_0} = \left(\frac{y}{a \bar{x}_1^{n/2}} \right)^{\frac{1}{n/2 + 1}}$$

where

$$y = 1 - \frac{E_f}{E} \frac{T_w}{T_f} \approx 1$$

In addition, it is generally true that

$$\frac{E_H}{RT_w} \gg m$$

$$\frac{E_f}{RT_f} \gg \frac{n+2}{2}$$

and, as a crude approximation valid over a limited range,

$$\bar{r} \sim b \left(\frac{T_w}{T_o} \right)^z \quad \text{where } z \gg 1$$

Substitution of these expressions into Eq. (22) in Appendix A leads to an approximate expression for the stability criterion in terms of burning rate and pressure. For the case where all surface-coupled reactions are heterogeneous, or pressure-sensitive, this expression is (in order to ensure stability):

$$\log (r/a) > \left[\frac{m + \frac{n}{\frac{n}{2} + 1}}{\frac{2y}{\frac{n}{2} + 1} - \frac{E_H}{E}} \right] \log P + \log \left[\frac{\frac{1}{2} \frac{C_S}{C_P} \frac{E_H}{E} \frac{E_f}{RT_o} \left(\frac{C}{A} \right)^{\frac{n}{2} + 1} \frac{H_H}{C_S T_o}}{\frac{2y}{\frac{n}{2} + 1} - \frac{E_H}{E}} \right] \quad (11)$$

If all surface reactions are pressure-insensitive, as might be the case in sub-surface decomposition, the expression becomes (in order to ensure stability):

$$\log \left(\frac{r}{a} \right) > \left[\frac{\frac{n}{\frac{n}{2} + 1}}{\frac{2y}{\frac{n}{2} + 1} - \frac{E_D}{E}} \right] \log P + \log \left[\frac{\frac{1}{2} \frac{C_S}{C_P} \frac{E_D}{E} \frac{E_f}{RT_o} \left(\frac{C}{a} \right)^{\frac{n}{2} + 1} \frac{H_D}{C_S T_o}}{\frac{2y}{\frac{n}{2} + 1} - \frac{E_D}{E}} \right] \quad (12)$$

Thus the stability criterion derived in the present report appears as approximately a straight line on the usual $\log r$ vs. $\log P$ plot. The

slope of this line is determined primarily by the effective order of the gas-phase and surface-coupled reactions. The intersect is determined mainly by the magnitude of the enthalpy release in the surface-coupled reactions per unit mass of reactant (H_H or H_O); when a relatively large portion of the total heat release occurs in this manner, the extent of the stable-burning regime is reduced. The converse result occurs when more of the heat release is in the gas phase. This behavior is illustrated in Figs. 13 and 14.

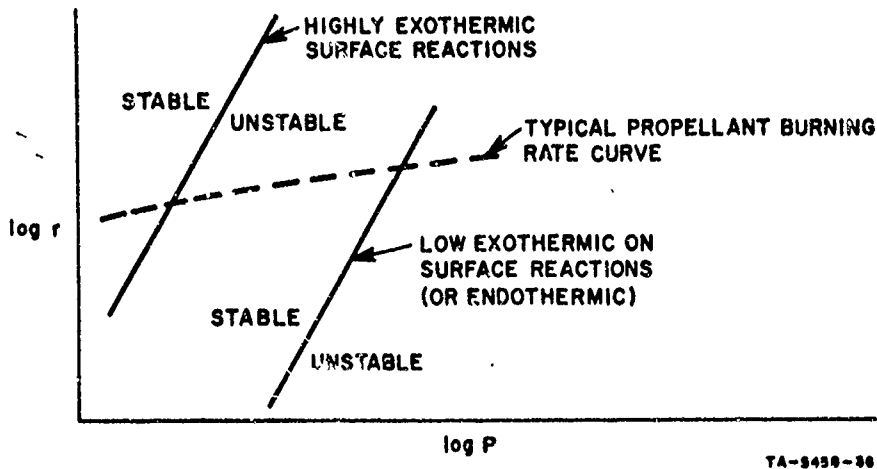


FIG. 13 PREDICTED STABILITY BOUNDS FOR PRESSURE SENSITIVE SURFACE REACTIONS

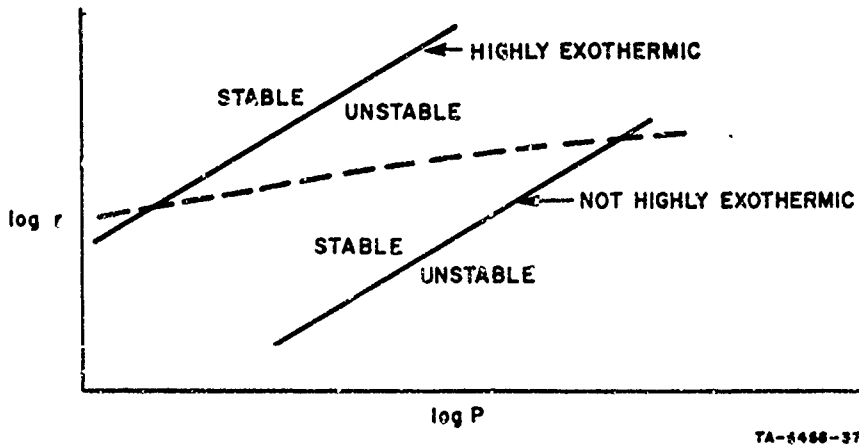


FIG. 14 PREDICTED STABILITY BOUNDS FOR PRESSURE INSENSITIVE SURFACE REACTIONS

As the figures show, the criterion implies that of two propellants having identical burning-rate curves but different formulations, the one having more highly exothermic solid-phase coupled reactions (such as an AP-based propellant) would be expected to operate unstably over a much wider pressure range than the one with less solid-phase heat release. This characteristic appears to be entirely consistent with the experimental observations made during the present program.

It should be re-emphasized that the approach outlined here is preliminary and approximate in nature. For example, a more rigorous examination of the same model would yield a somewhat more complicated stability criterion; even with the present simplified analysis there would be a slight curvature in the plot of the criterion on a $\log r$ vs. $\log P$ graph, if the criterion were transformed to the r - P plot without approximation. However, the approximations employed here are quite consistent with the accuracy to which the pertinent parameters can be measured, so that further extensions and refinements of the model may be of greater value in future studies than refinements in the mathematical treatment of the present model. The present work suggests that a relatively fundamental approach to the solid propellant combustion problem may ultimately define and clarify significant mechanisms and interactions that heretofore have been overlooked.

D. Experimental Studies to Correlate Stability Criteria with Ballistic Design Parameters and Propellant Microstructure

It will be recalled that in our previous studies an attempt was made to correlate the observed stability criterion found for ammonium perchlorate-based propellants with a combustion model based on critical mixing parameters of a diffusion flame which is believed to be present at the burning surface of composite propellants. A relationship was developed from similitude studies based on simple turbulent mixing model proposed by Bittker.¹⁰ It was suggested by our analysis that instability was characterized by a constant relationship between the wave travel time, t_w , in the motor and the characteristic combustion time for mixing, t^* . This ratio $\frac{t^*}{t_w}$ is defined by the following equation:

$$\frac{t^*}{t_w} = \frac{\alpha M^* s c}{J \rho_s R 2l} \frac{P_T}{r_T T^*} \quad (13)$$

where α = mixing parameter¹⁶
 J = intensity of turbulence¹⁶
 M^* = mean molecular weight of reacting species
 s = source spacing
 c = speed of sound
 ρ_s = density of solid propellant
 R = gas constant
 l = motor length
 P_T = threshold pressure
 r_T = threshold burning rate
 T^* = initial temperature of reacting species
 (Note $T^* \simeq T_{\text{surface}}$)

It is noted that the wave travel time criteria predict that for different propellants in the same scale motor the stability bound would be defined by a line with a slope of approximately unity. The corrections for known variation in surface gas temperature and other propellant parameters reduced the slope slightly and brought it into line with the experimental stability bound data.

It was apparent from equation (13) that two critical parameters in defining a similitude criteria for instability were the source spacing s (a function of oxidizer particle size or specific surface) and the motor length l . In view of these facts two sets of experiments were planned; in one several combinations of motor length and propellant composition were test fired, and in the other, two propellants with matched ballistics (burning rate) were prepared with the largest mean particle size difference that could be satisfactorily formulated into propellants.

To determine if design factors such as motor length would shift the critical stability line,¹⁵ several motors, 5 inches x 80 inches long with a 3 inch-diameter perforation, were test fired. Following standard

procedure, Kistler gages located at the head end were used to monitor the pressure response and multiple pulses were used to perturb the motor over the pressure range of interest in order to find the critical pressure for instability. The data for the 80-inch motors are plotted on our original instability diagram for 5-inch x 40-inch motors in Fig. 15.

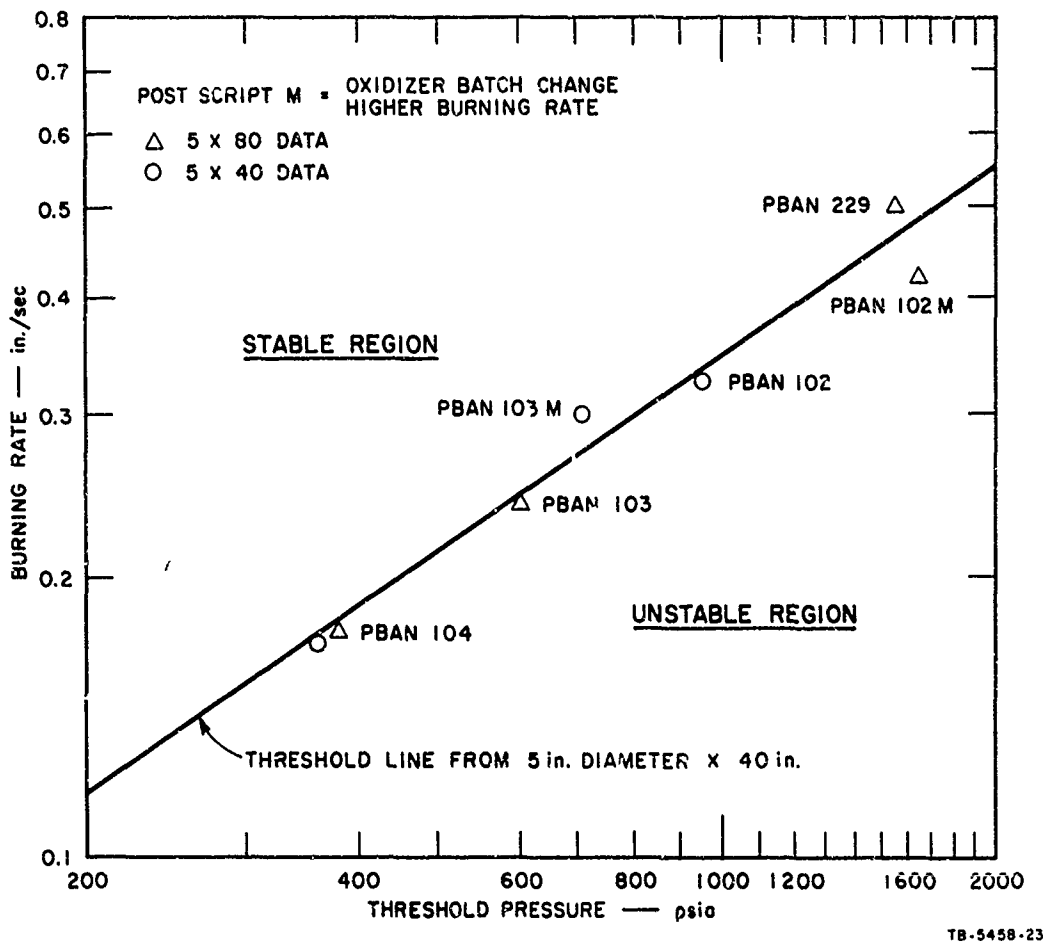


FIG. 15 STABILITY BOUND FOR 40-INCH AND 80-INCH LONG MOTORS

Since all of the 80-inch-motor data points fall closely about the stability line for the 40-inch motor, the obvious conclusion is that this variation in length did not significantly alter the stability characteristic of our AP-containing propellants.

The two propellants selected for the study of oxidizer particle size (source spacing) had lithium fluoride and strontium carbonate added to counter the rate variations produced by the oxidizer grind variations. The formulations are given in Table I. The strand burning rates are shown in Fig. 16. When tested for critical threshold pressure, PBAN 244 (with a surface area of $3015 \text{ cm}^2/\text{cc}$) gave 320 psi, while PBAN 284 (surface area of $1149 \text{ cm}^2/\text{cc}$) gave 400 psi. This appears to be contrary to prediction, but it is not considered to be at all significant because the burning rate curves appear to parallel the instability line at these low pressures. It is concluded that oxidizer surface area variations of the type normally encountered in propellant formulations

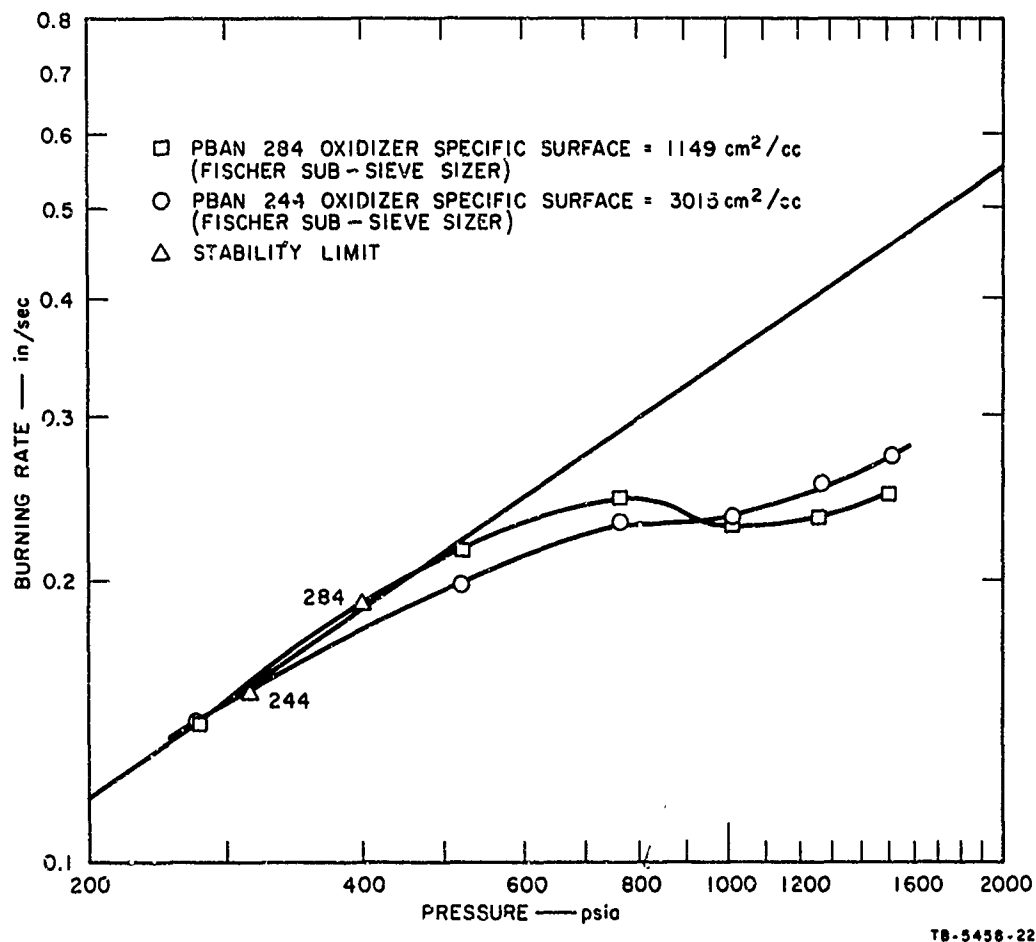


FIG. 16 BURNING RATE AND STABILITY DATA FOR PROPELLANTS WITH MATCHED BALLISTICS BUT DIFFERENT OXIDIZER PARTICLE SIZE

play a minor role in finite amplitude instability. The chief role of oxidizer particle size appears to be in its effect on burning rate, the major correlating parameter.

1. Influence of Fuel/Binder Characteristics on Instability

It had been observed in previous experimental studies¹³ that instability was enhanced by a burning rate apparently associated with a reduction in flame temperature promoted by addition of either an endothermic burning rate catalyst (LiF) or a fuel-rich oxidizer-fuel ratio. In view of the relevance of propellant thermochemistry to development of a suitable combustion model, it was decided to examine the influence of binder pyrolysis characteristics on the incidence of axial stability. Polyurethane and polybutadiene acrylonitrile-based propellants were therefore compared at two loadings of ammonium perchlorate. The loadings selected, 80% and 75% by weight, are representative of many aerospace propellants.

The experimental results showed that the oxidizer-rich propellants (20% fuel) based on both binder systems were unstable at the pressure level predicted by the AP stability data previously obtained. At the higher level of fuel (25%), it was found that the polyurethane-based propellant PU 108 was unstable at the predicted pressure of 280 psia. The PBAN binder, however, could only be driven unstable at a pressure of 685 psia, some 400 psi higher than predicted.

In comparing these results it must be noted that:

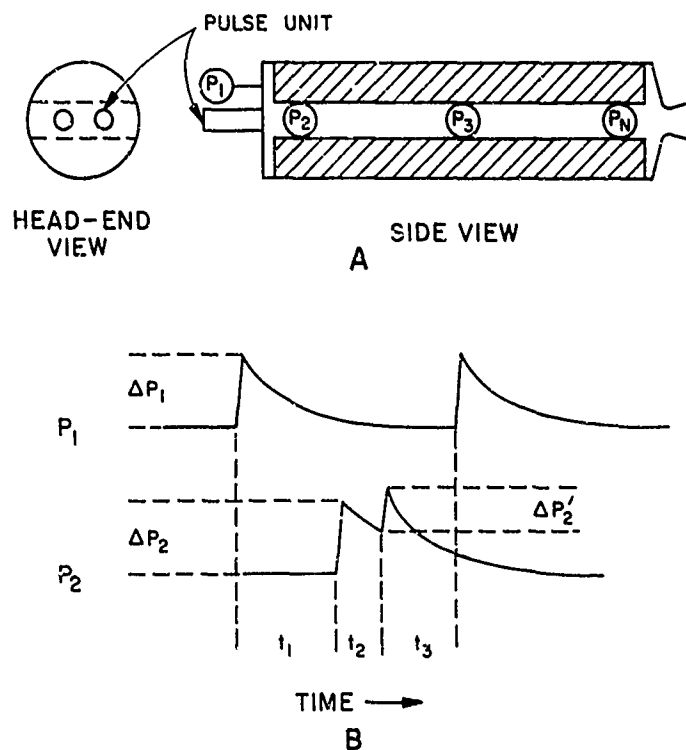
1. AP is more soluble in the PU binder.
2. PU-based propellants appear to develop a greater degree of instability as measured by the amplitude and the D.C. pressure level during periods of instability.
3. PU binders are more readily pyrolyzed than PBAN binders.

These facts appear to be consistent with the theory developed in Section III(E); the less highly over-all exothermic surface reactions promote stability.

Further study of the influence of binder characteristics on instability awaits a more complete development of the stability criteria outlined in Section III(E). These criteria will be tested using all available data before additional experiments are planned.

2. Loss and Gain Processes During Axial Mode Traveling Wave Instability

It was recognized that the growth processes and loss mechanism of a traveling wave type of instability could be examined by measuring the amplitude and velocity of the wave as it propagated up and down a rocket motor. Motors of various lengths with a regressively burning rectangular perforation were selected for this study and after being driven unstable by a pulse, the wave travel up and down the grain was monitored by high frequency pressure transducers located at stations on the side and at the head-end of the rocket as shown in Fig. 17.



TA-5458-28

FIG. 17 SCHEMATIC LAYOUT AND DATA ANALYSIS PROCEDURE FOR AXIAL STATION PROBING OF TRAVELING WAVES IN ROCKET MOTORS

The transducers selected were Kistler Model 601 and/or 601A piezo-electric pressure gages whose outputs were short-coupled to charge amplifiers (Kistler Model 566 and/or 504). The amplifier outputs were recorded on magnetic tape. The gages had to be protected from the high heat flux during instability and accordingly, water cooled mounts (Model 629) were used. The decoupling of the gage through the mount reduced the absolute pressure response to 10 kc. The time-averaged chamber pressure was monitored with a strain gage type transducer (Taber Model 206) which was recorded on the oscillograph.

The propellant used in the rocket motors was the 80% APC - 20% PBAN system, PBAN 103. For the tests the motor length was varied from 82 inches down to 15 inches. All motors were operated at an initial chamber pressure of 1100 to 1200 psi and were pulsed shortly (100 to 300 msec) after the appropriate steady state chamber pressure was reached. This was accomplished by the use of a pressure sensor which activated the time-delay unit inserted to regulate the firing of the pulse.

E. Data Reduction

The data from all channels were played back from the tape into an oscilloscope which was equipped to handle six channels. Values for travel time (t_n) between stations and the pulse amplitude (ΔP) at each station were taken from the oscillograms as indicated in Fig. 17.

Port-area to throat-area ratio (j) was calculated using the assumption that the characteristic velocity (C^*) was invariant under the test conditions. Using the pressure-time integral as a measure of propellant mass consumption, the space-averaged port area at a given time could be readily computed.

The gas velocity in the grain port at nozzle was calculated using the standard ballistic relations:

$$v = \frac{\dot{w}}{\rho A_p} = \frac{g A_t P_c}{C^* \rho_g A_p}$$

The theoretical velocity of sound for this propellant system at the nominal chamber pressure of 1250 psi was calculated using theoretical values for γ and ρ .

$$A^* = \sqrt{\frac{\gamma P}{\rho}} = 3180 \text{ ft/sec.}$$

The observed values of the shock velocities and other pertinent data are listed in Table III; shock velocities (average values are given) based on cycle time from the head-end pressure transducer. The influence of stream velocity on the shock characteristics with and against the stream could not be exactly determined because the shock strength increases during transit along the burning surface.

Table III
SUMMARY OF EXPERIMENTAL DATA RELATING TO TRAVELING WAVE PROPAGATION
IN ROCKET MOTORS OF VARYING LENGTHS

Test No.	Length (inches)	A_t (in ²)	J	f (cps)	\bar{v} (ft/sec)	\dot{w} (lb/sec)	v (ft/sec)
6	40	0.710	5.33	466	3100	7.00	360
37	23	0.386	13.85	803	3075	3.73	124
38	40	0.707	9.15	464	3095	6.03	212
40	82	1.539	4.3	238	3250	14.20	445

It will be seen that in any particular motor a significant increase in wave strength occurs as the wave propagates along the grain. In Fig. 18 the amplitude of the wave front versus station during travel to and from the head end along the port is shown for a 5-inch x 80-inch regressively burning slab motor.

Oscillograms provided by tape playbacks were used to obtain the instantaneous pressure increases at each measuring station along the motor. These pressure changes at each station are plotted in Figs. 19(a-d) for some typical tests using a range of motor lengths. In Fig. 20 we reproduce the pressure vs. time history for up to 3 sec. during the unstable burning of a 5-inch x 40-inch slab motor. (It should be noted

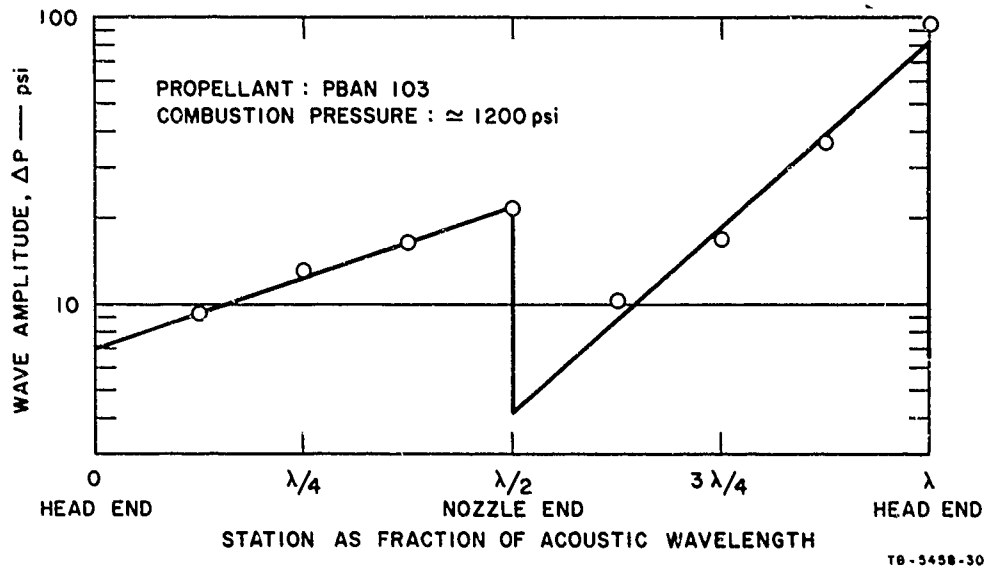


FIG. 18 OBSERVED PEAK PRESSURE AMPLITUDE OF THE TRAVELING WAVE DURING PROPAGATION IN A 5-INCH DIA. \times 80-INCH LONG ROCKET MOTOR BURNING PBAN 103

that the grain design used burns regressively so that the burning surface area decreases throughout the run and this results in the pressure ultimately entering a stable regime.) A 15-inch motor was also tested but it did not go unstable; in fact, it was possible to track the pressure perturbation for only one cycle before it dampened and stable burning continued. The Kistler gage responses at $1/4$, $1/2$, and $3/4$ stations down the grain are shown in Fig. 21 for this test.

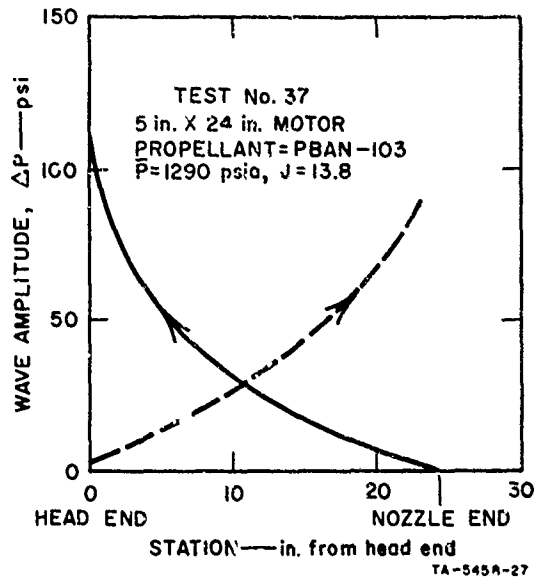


FIG. 19 OBSERVED PEAK PRESSURE AMPLITUDE AS A FUNCTION OF MOTOR LENGTH DURING TRANSIT UP AND DOWN THE MOTOR

(a) 24-INCH MOTOR

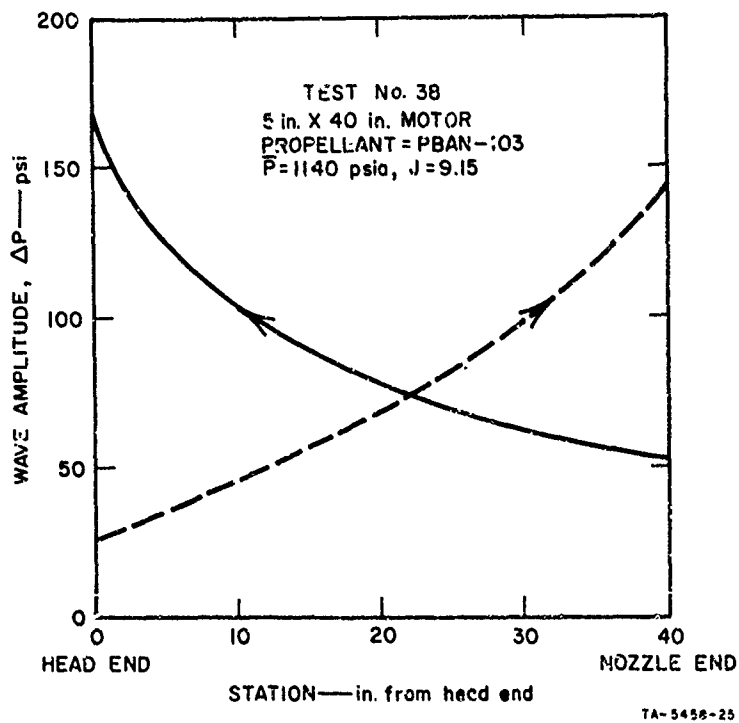


FIG. 19 (b) 40-INCH MOTOR

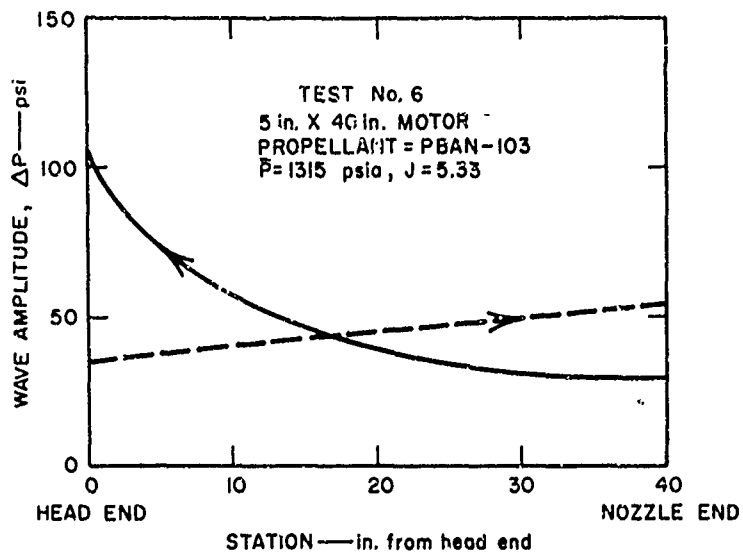


FIG. 19 (c) 40-INCH MOTOR

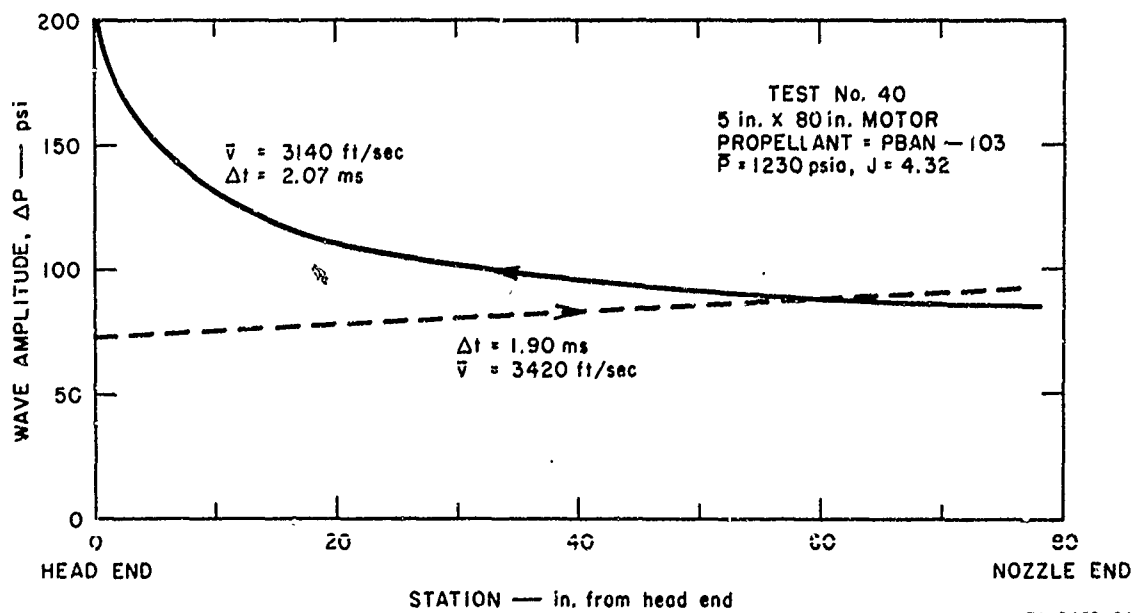
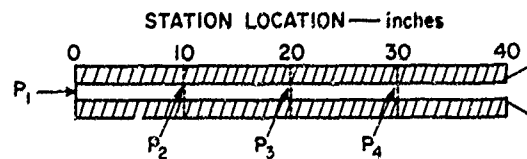
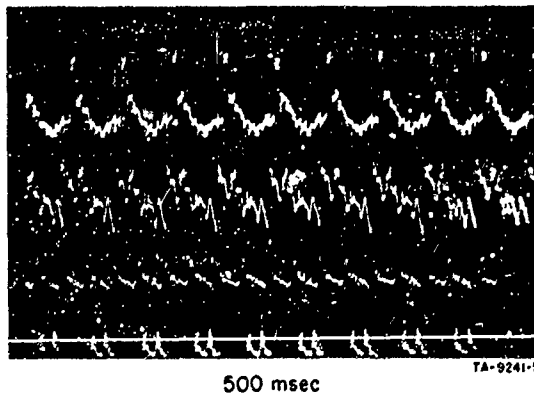
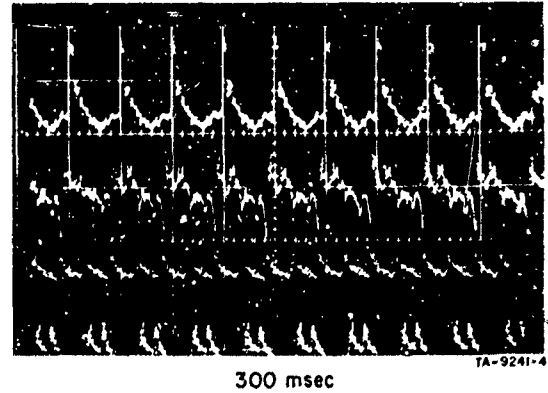
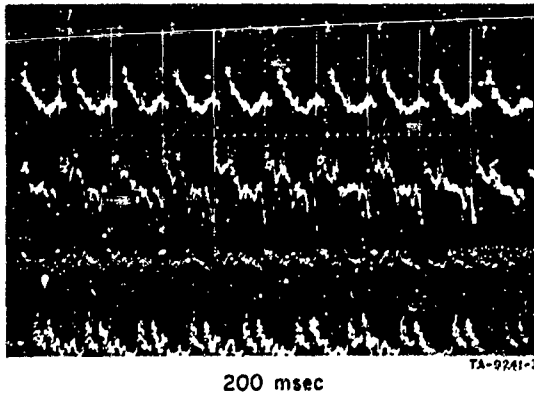
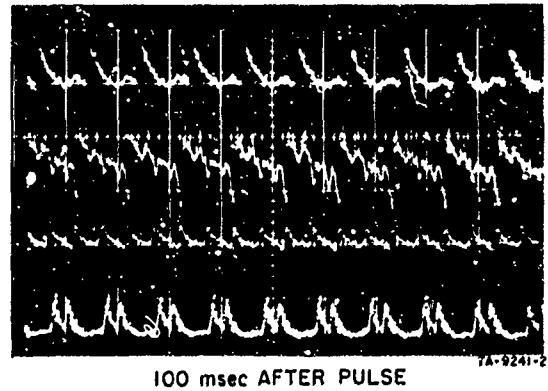
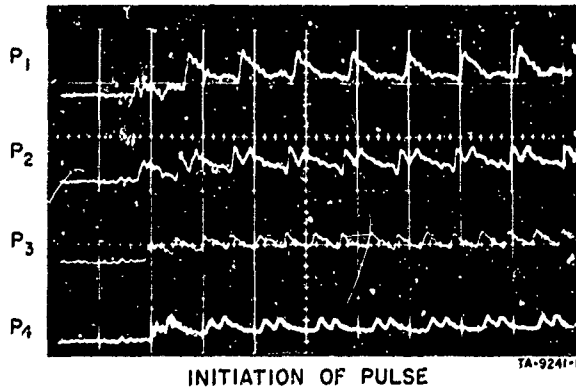


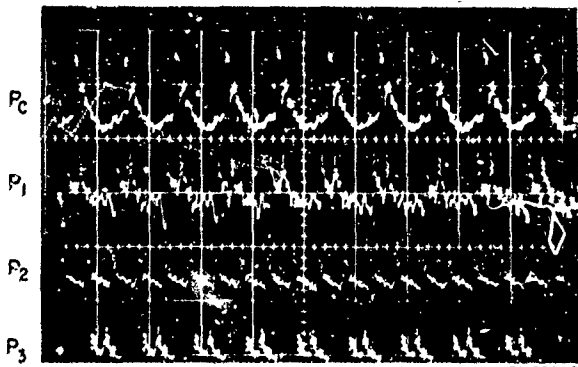
FIG. 19 (d) 80-INCH MOTOR



NOTE:

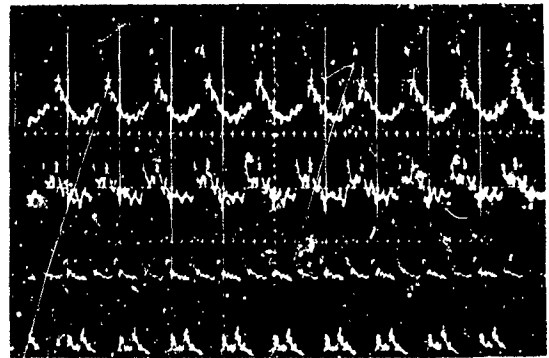
1. 2 msec PER HORIZONTAL DIVISION
2. 300 psi PER VERTICAL DIVISION
3. ALL TIMES FROM INITIATION OF INSTABILITY

FIG. 20 TRAVELING WAVE PRESSURE/TIME HISTORY FOR 40-INCH LONG MOTOR AT VARIOUS TIME INTERVALS



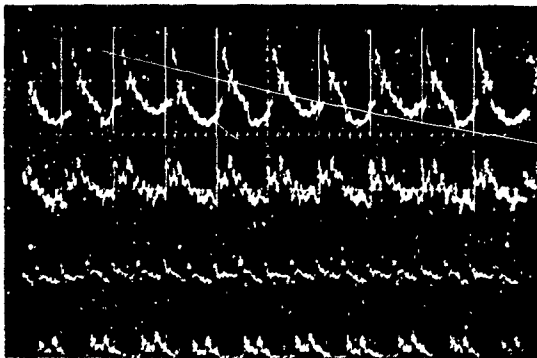
1,385 msec AFTER PULSE

TA-9241-6



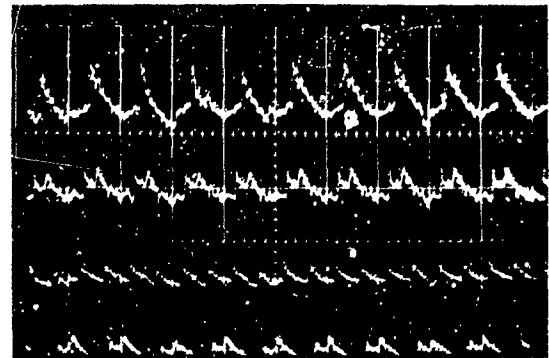
1,500 msec

TA-9241-7



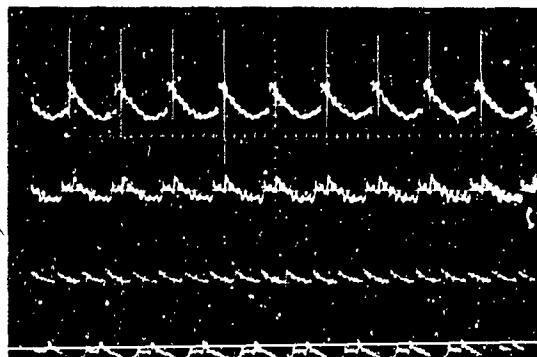
2,330 msec

TA-9241-8



2,500 msec

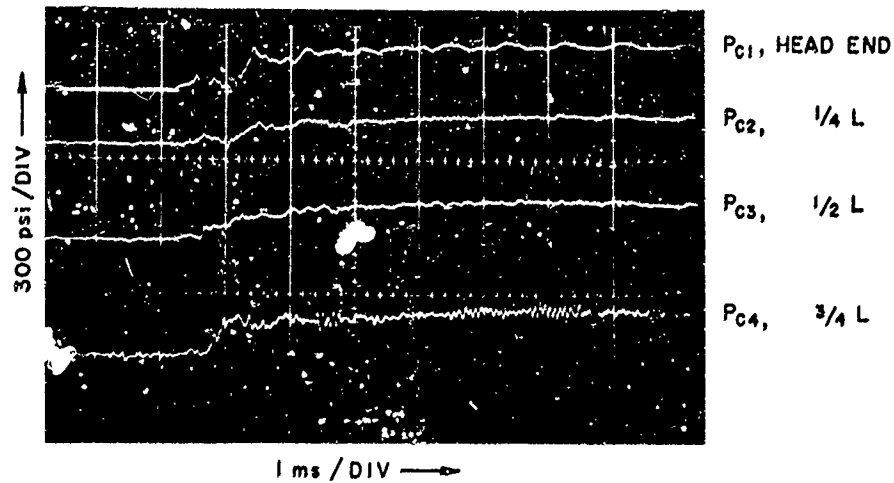
TA-9241-9



3,000 msec

TA-9241-10

FIG. 20 (Continued)



TA-5458-55

FIG. 21 MULTI-STATION PRESSURE RESPONSE OBSERVED
IN A 15-INCH LONG MOTOR ON PULSING

F. Data Interpretation

The increase in pressure that occurs in a traveling wave front going from the nozzle end to the front end and back is plotted in Fig. 22 on a normalized basis for a series of rocket motors varying in length from 24 to 80 inches. It will be noted that the wave strength appears to increase during transit along the grain and to suffer very significant losses in amplitude on reflection at the ends. It is surmized that energy is gained from coupling of the flow disturbances with the combustion process at the surface of the propellant due to pressure coupling and/or turbulent mixing (erosive coupling). The good straight line correlation for pressure wave growth toward the nozzle end suggests that an exponential growth is occurring which may be represented by a relation such as:

$$dP = \beta \exp^{\alpha x / \ell}$$

where dP = instantaneous increase in pressure caused by wave passage
over gage face

α = growth constant

x = distance from head end

ℓ = length of motor

(Note that $2 \ell = \lambda$ (one wavelength))

β = pressure coefficient

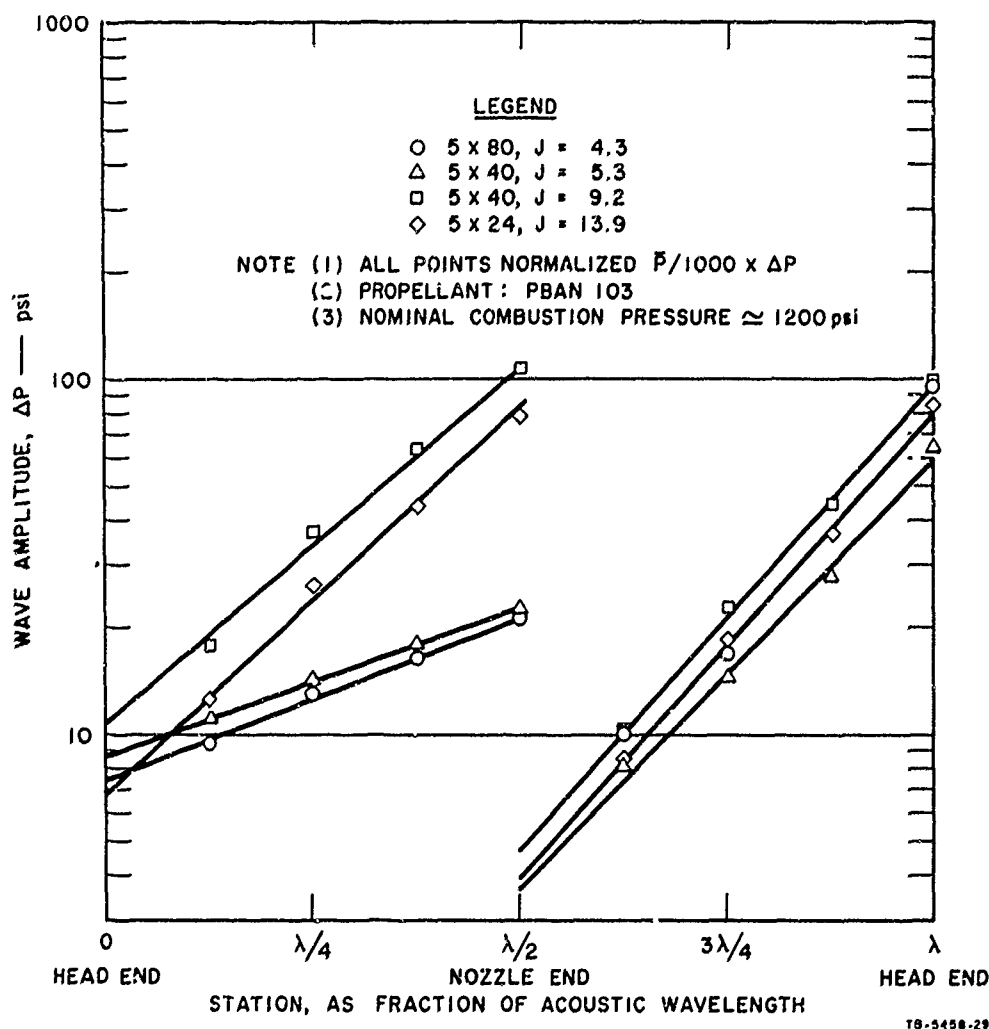


FIG. 22 NORMALIZED GROWTH CHARACTERISTICS FOR TRAVELING WAVES OBSERVED IN ROCKET MOTORS OF DIFFERENT LENGTHS

As the wave is reflected from the nozzle there is a loss in energy which caused a drop in dP. This energy loss comes from two factors. First, mass and heat are lost from the nozzle opening. Second, the impact of the high speed wave upon the solid portions of the nozzles causes high rates of heat transfer to the nozzle, and this too subtracts energy from the wave.

Our evidence for high rates of heat transfer at the nozzle comes from early experiments in which thermal shock was found to cause failure of a dense carbon nozzle and a softer carbon had to be substituted. The softer carbon always shows high erosion rates on internal surfaces when used in a motor operating in an unstable pressure regime.

After the wave amplitude attenuation caused by nozzle losses, gain mechanisms predominate during transit back to the head end and the pressure gain in the wave front again is described by a typical exponential growth equation. The gain against the mean flow is more pronounced than for wave travel with the mean flow from the head end to the nozzle. Upon impacting the head end, the wave again loses energy through heat transfer mechanism and there is a loss in wave strength. This high rate of heat transfer upon reflection at the head end is again manifested by severe erosion of the face of the pulse head.

On examining the sawtooth wave structure obtained when the data are plotted on semi-log paper, we note that the growth constant for propagation against the mean flow appears to be constant for all motors, while with the mean flow the growth constant appears to depend on motor operation and design parameters. This difference in behavior can be explained on the basis that the admittance of the head end is invariant in all motors but that of the nozzle is dependent on the nozzle design and the mean flow field near the nozzle.

In addition to our pressure measurements along the length of the rocket motors described previously, it was possible to also measure the

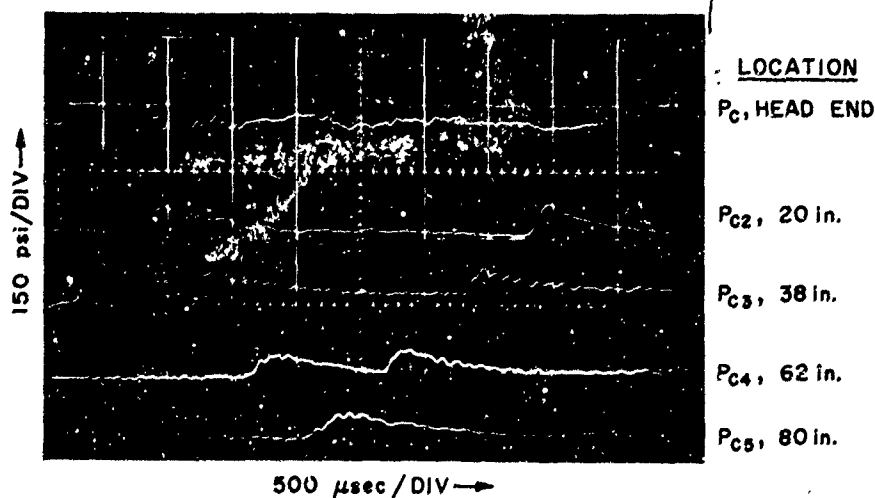


FIG. 23 TYPICAL OSCILLOGRAM USED FOR COMPUTATION OF THE VELOCITY OF THE TRAVELING WAVE IN THE 80-INCH LONG ROCKET MOTOR

wave velocity from the arrival times at each of the monitoring stations. The data for the 80-inch motors was obtained from oscillograms such as that shown in Fig. 23. The wave velocities obtained in this manner are thus those averaged over the distance between pressure gages. These average velocities are plotted for three typical cycles of the wave as a step curve in Fig. 24. An attempt to visualize the wave shape of the velocity profile up and down the rocket motor is shown by the dotted line in Fig. 24. It will be observed that:

1. When wave travel is toward the nozzle a maximum velocity is observed near the three-quarters station on the way to the nozzle.
2. Upon reflection from the nozzle a velocity increase is observed.
3. When wave travel is from the nozzle to the head there is a minimum velocity near the quarter station on the way to the head end.
4. Upon reflection from the head end, the velocity appears to decrease.

The picture of the velocity profile up and down the motor is somewhat distorted, because it is only possible to measure average velocity between stations and the discrimination is not yet as good as it should be since it is dependent on available transducers. However, all measurements on 80-inch motors suggest that the description given by Fig. 24 is correct. Due to lack of time resolution in short motors, our experimental study is limited to the 80-inch motor.

In Fig. 25 the station relations for the pressure increment and velocity increment of a single cycle are visualized. It is apparent that the growth characteristic of the pressure wave does not bear a uniform phase relationship with velocity. As the wave approaches the head end, the station variant velocity is in phase with pressure; after reflection, it is also in phase. On passing the quarter wavelength, the station variant velocity changes so that it is 180° out of phase with

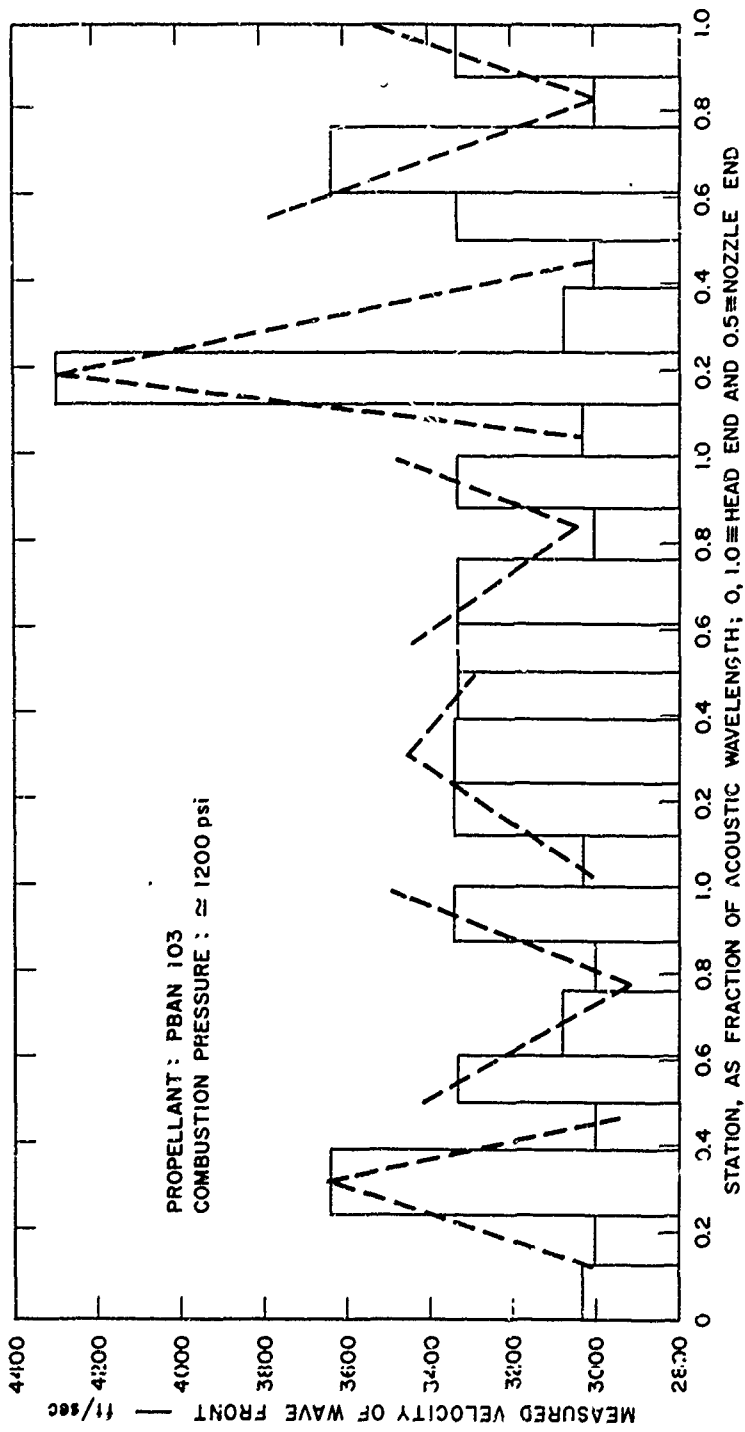


FIG. 24 VELOCITY PROFILE OF TRAVELING WAVE AS DETERMINED BY ARRIVAL TIME OF PRESSURE TRANSDUCERS

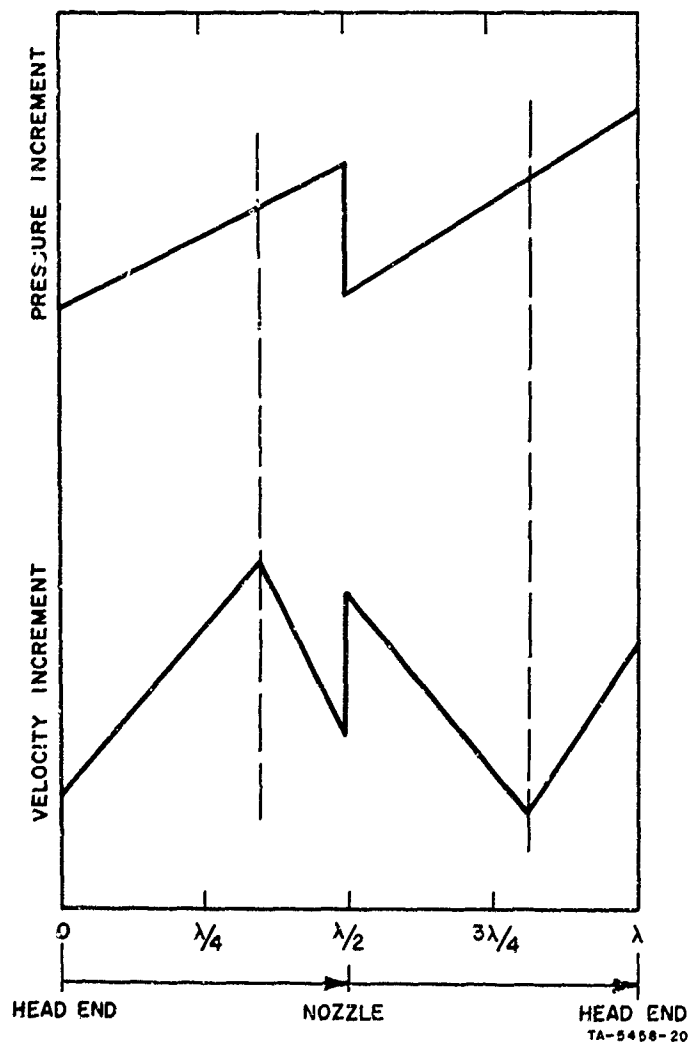


FIG. 25 VISUALIZATION OF PHASE RELATIONSHIP BETWEEN PRESSURE AND VELOCITY OF A TRAVELING WAVE IN 80-INCH LONG ROCKET MOTOR

the pressure, as predicted from traveling acoustic wave theory. After reflection from the nozzle end velocity continues to be out of phase with pressure until at about the $3/4$ wavelength station it apparently comes into phase.

There is some evidence that the wave pressure amplitude may have a contribution from a standing acoustic wave: similarly, the velocity profile observed has at certain periodic times some of the characteristics anticipated for a combination of the acoustic velocity field of a standing wave and the mean flow field in the rocket motor. As yet inadequate resolution in our velocity measurement precludes a rigorous numerical analysis of the finite amplitude traveling wave observed.

Future work will seek to identify the specific growth mechanism occurring as the wave propagates and to examine further the loss mechanism occurring on wave reflection at the ends. It is hoped that studies of different propellants may elucidate the dependence of the growth constant on specific chemical processes.

V SUMMARY DISCUSSION

A. Compositional Factors

The experimental results have shown two distinct trends; one is the association of finite-amplitude traveling wave combustion instability in composite propellants with the presence of ammonium perchlorate; the other, that in the case of double-base propellants this type of instability appears to be associated with a thick fizz burning zone.

B. Composite Propellants

In our experimental study of composite propellants a unique combination of propellants possessing different ballistic behaviors and containing different oxidizer binders and other additives have been investigated. Specifically the study was concerned with the incidence of finite amplitude traveling wave instability induced by pulsing the chamber pressure. Data have been obtained principally by using rocket motors 40 inches and 80 inches long by 5 inches in diameter, and it has been shown again that propellant burning rate is, in the case of AP-containing propellants, the most important parameter with which to correlate instability behavior. The data are summarized in Fig. 26 for propellants which have been formulated to provide maximum energy (consistent with large scale processability); the propellants examined have chiefly used a hydrocarbon binder (polybutadiene acrylic and acrylonitrile terpolymer).

It will be noted that all AP-containing propellants with a burning rate vs. pressure relationship extending to the regime to the right of the stability bound are liable to operate unstably. The oxidizers KP, LiP, and AN were found to be associated with stable combustion. A qualitative explanation of the observed behavior of AP-containing propellants suggests that stability in potentially unstable propellants is associated with the rate-controlling low activation energy reaction between HClO_4 and fuel pyrolysis fragments in the premixed flame. This reaction releases more energy than the AP monopropellant flame and

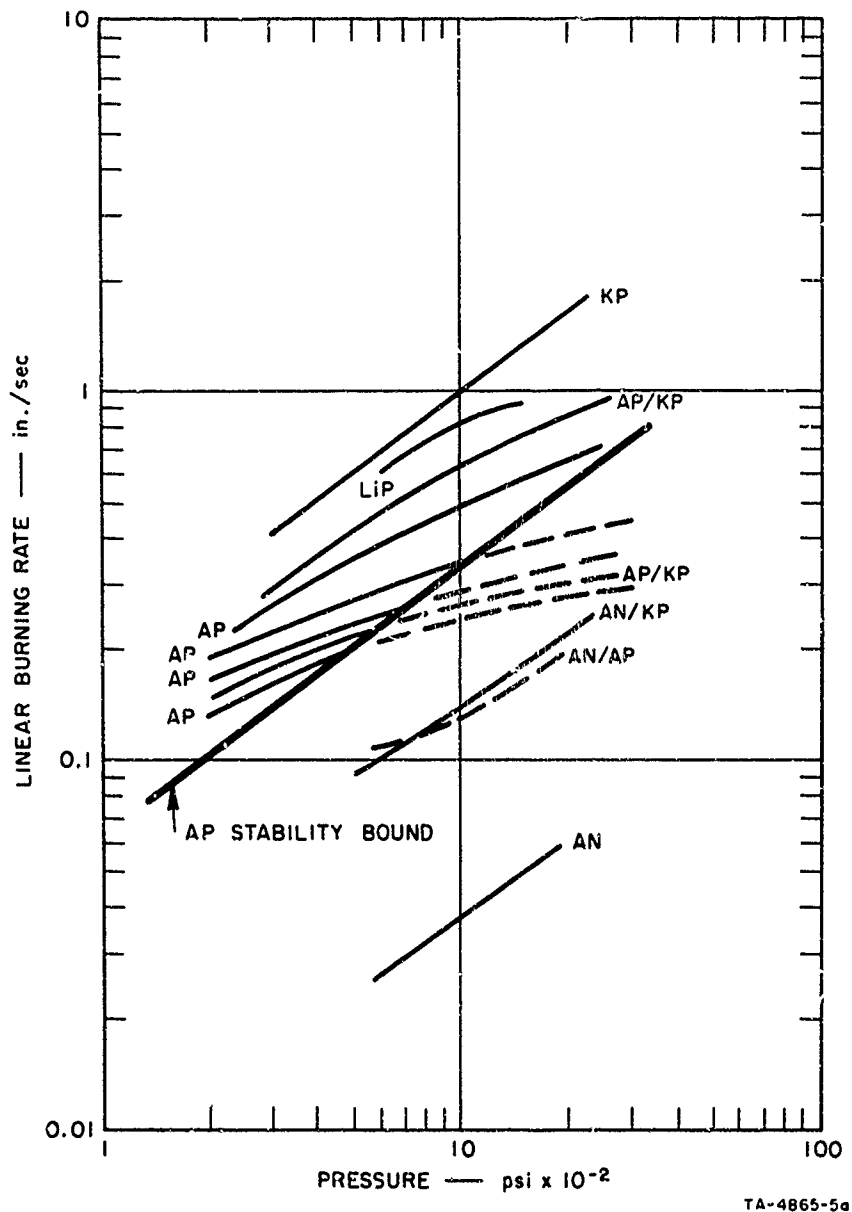


FIG. 26 INFLUENCE OF BURNING RATE AND COMPOSITION ON FINITE AMPLITUDE TRAVELING WAVE INSTABILITY; SOLID LINE STABLE REGIME, DOTTED LINE UNSTABLE REGIME FOR 5-INCH x 40-INCH MOTOR

consequently the propellant burns faster than pure AP. At higher pressure it appears that the premixed flame becomes a modified diffusion flame in which the over-all mass burning rate is suppressed because of a progressive change of the relative amounts of heat transfer back to the oxidizer and the pyrolyzing binder. The energy release profile and temperature profile in the combustion wave govern the mass burning rate of the propellant; these profiles would appear to be controlled primarily by the enthalpy changes associated with pyrolysis of the binder, decomposition of the oxidizer, and specific surface-coupled reactions such as the monopropellant AP flame.

It is possible that at high pressure an imbalance in the heat transfer back to oxidizer and fuel components occurs; augmented heat transfer back from the fully burned combustion products may then arise due to turbulent mixing associated with flow perturbations; this in turn can lead to the transient accelerated reaction of partially reacted combustion products and perhaps in certain cases to an over-all increase in the mass rate of burning.

In the case of AP propellants, in contradistinction to KP propellants, it is noteworthy that the mass burning rate can be accelerated or depressed by the addition of combustion catalysts. Catalysts such as iron oxide appear to increase the temperature gradient at the surface, which results in an increase in burning rate; it is presumed that the catalyst promotes either the gas-phase reactions near the surface or condensed-phase reactions. It can be postulated that promotion of the condensed-phase reactions can result in a lower surface temperature for a given decomposition rate or a high rate of decomposition at a given temperature. The experimental studies performed in this program suggest that increase of burning rate by either catalysis or particle size control promotes stability by raising the level of heat transfer back to surface. Consequently under these conditions heat release in the surface becomes less significant from the standpoint of the over-all decomposition process.

The exact role that catalysts which accelerate burning rate play in the flame microstructure is still open to conjecture; in many instances

the catalyst functions very effectively even though it is dispersed in an ablative coating of fuel. It is possible that the catalyst functions in two roles; it promotes certain oxidative reactions, and the localization of energy release generates additional local turbulence which also promotes the over-all combustion reaction. The burning rate depressants may also function in two ways; they may reduce the temperature gradient near the surface and they may also quench the AP monopropellant flame. Certainly the unique behavior of lithium fluoride as a rate depressant suggests that it modifies AP decomposition.

It is noteworthy that similitude studies based on mixing criteria in the granular diffusion flame, while predicting the observed pressure-burning rate relationship, did not scale satisfactorily. This suggests that the driving of this type of combustion instability is not associated directly with the diffusion flame at the surface; this supports strongly the idea that the unexplained low burning rate of the AP propellants concerned is of primary importance.

C. Double-Base Propellants

The observed behavior of the double-base propellants suggests that finite-amplitude traveling wave instability is associated with the relatively thick primary reaction zone observed at low pressures and low burning rates.

The traveling wave instability is sustained by the shock pressure (and associated temperature increase) promoting the reactions which are only partially complete near the surface of the propellant; again turbulent mixing behind the wave front may also promote the combustion reactions.

It is conceded that an extensive study of double-base formulations has not been possible, but the gain mechanism suggested--reaction promotion by the shock front--is entirely consistent with well-established concepts of the steady-state burning of double-base propellants.

D. Stability and Scaling

The studies performed on traveling wave amplitude growth during transit along the grain have shown that a simple exponential growth relationship appears to hold for motors of different sizes. Cyclic growth is, however, modified by very heavy losses occurring on reflection at the nozzle and head ends.

It has been found that motors of low aspect ratio are inherently stable; no simple reason can be found to explain this fact. It is perhaps related to losses sustained on reflection at the nozzle end. The nature of the traveling shock wave and associated wake structure may also be of importance; a complex interaction of the reflection of the primary shock with wake reflection may also attenuate the shock. (The nature of the shock pattern is briefly discussed in Appendix B.)

The complex pressure and velocity characteristics determined for the shock indicate that a satisfactory model accurately predicting stability scaling factors related to geometry may be quite formidable. Fortunately the work to date suggests that propellant ballistics can be chosen in such a manner that unstable regimes can be avoided.

E. Analytical Models

It is expected that the combustion model being developed will make it possible to predict propellant response to flow perturbation on the basis of the chemistry of the propellant constituents.

Some success has already been achieved in predicting stability on the basis of the energy release profile within the combustion wave. It appears that energy release at the surface or in surface-coupled gas phase reactions may promote instability. The model, while an improvement on previous quasi-steady treatments, can be further improved by a more sophisticated approach involving chemical kinetic consideration of surface and response-coupled reactions.

VI CONCLUSIONS AND FUTURE WORK

The principal conclusions reached in our study are:

1. Combustion reactions associated with the presence of ammonium perchlorate rather than macro-ballistic behavior have been identified as a major contributing cause of finite amplitude traveling wave axial instability in composite propellants.

2. Incipient low frequency (200 - 800 cps) traveling wave type instability can be avoided by selecting propellants inside a given burning rate vs. pressure regime.

3. Stable operation of double-base propellants appears to be enhanced at elevated pressures.

4. An analytical combustion model being developed appears to be capable of explaining observed propellant behavior on the basis of propellant chemistry.

Future work will be directed primarily toward elucidating loss mechanisms in wave propagation in rocket motors. Emphasis will also be given to further developing the analytical model and identifying the exact nature of critical processes in the construction of ammonium perchlorate.

ACKNOWLEDGEMENT

The assistance of Jack Smith, project technical supporting staff coordinator, is gratefully acknowledged.

NOMENCLATURE*

- a = frequency factor in Arrhenius law (Eq. 2)
 A_t = throat area
 b = coefficient in empirical burning rate law, $r = bP^n$
 C = constant defined by Eq. (7)
 C_1 = constant defined by Eq. (22)
 C_2 = constant defined by Eq. (23)
 C_p = specific heat capacity of the gas
 C_s = specific heat capacity of solid
 E = activation energy for vaporization of interface (Eq. 2)
 E_D = activation energy for pressure-insensitive solid-phase decomposition reactions (Eq. 9)
 E_f = activation energy for gas-phase reaction (Eq. 7)
 E_H = activation energy for heterogeneous or pressure-sensitive solid-phase reactions (Eq. 8)
 f = frequency
 h_{g_w} = energy carried into gas phase with the vaporizing propellant per unit mass
 h_{s_w} = energy carried by convection from the unreacted solid phase per unit mass
 H_D = heat release (positive) per unit mass propellant in decomposition reactions (Eq. 9)
 H_H = heat release (positive) per unit mass propellant (at a reference temperature and pressure) in heterogeneous reactions (Eq. 8)
 J = port to throat area ratio
 K = thermal diffusivity (of solid unless otherwise specified) = $k/\rho_s C_s$
 k = thermal conductivity

*Unless otherwise noted, equation numbers refer to Appendix A.

NOMENCLATURE (Continued)

- L = heat of vaporization per unit mass of propellant
 m = order of heterogeneous reaction (Eq. 8)
 n = order of gas-phase reaction (Eq. 7); also pressure exponent in empirical burning rate law
 P = chamber pressure
 Q_D = energy released from solid-phase surface reactions
 Q_H = energy released (gas-phase coupled) from heterogeneous decomposition reactions
 Q_r = heat of reaction per unit mass of reactant in the gas phase reaction
 R = gas constant
 r = burning rate
 T = temperature
 t = time
 v = gas velocity in grain port at nozzle end
 \bar{v} = mean velocity of shock front
 w = mass flow rate (nozzle end)
 x = distance into the propellant from its surface
 β = constant defined by Eq. (26)
 e = amplitude of pressure oscillation (Eq. 24)
 $\epsilon_{r,w}$ = fraction of total mass flux at the wall associated with reactant (nearly unity at the wall)
 $\theta_H,$
 θ_D = defined on p. 33
 λ = constant defined by Eq. (10) in text
 ρ_s = density of solid propellant
 τ = relaxation time

Subscripts

- DL = lower deflagration limit
 f = gas phase flame
 g = gas phase

NOMENCLATURE (Concluded)

- o = conditions at $x \rightarrow \infty$
s = solid phase
w = conditions at the wall (gas-solid interface)

Superscripts

- ($\bar{\quad}$) denotes value of quantity prior to pressure disturbance
($\tilde{\quad}$) denotes difference between perturbed and unperturbed value, divided by unperturbed value; $\tilde{r} = (r(t) - \bar{r})/\bar{r}$.

REFERENCES

1. L. A. Dickinson, Command Initiation of Finite Wave Axial Combustion Instability in Solid Propellant Rocket Motors, *ARS Journal* 32, 643 (1962)
2. M. Summerfield, G. S. Sutherland, M. J. Webb, H. J. Taback, and K. P. Paul, Burning Mechanism of Ammonium Perchlorate Propellants, *Progress in Astronautics and Rocketry*, Vol. I, Academic Press, pp. 141-182
3. M. Barrere, and A. Williams, Analytical and Experimental Studies of the Steady-State Combustion Mechanism of Solid Propellants, Office National D'Etudes et de Recherches Aerospatiales, Chatillon-sous Bagneux (Seine), T. Pub. No. 240 (1965)
4. J. Powling, The Combustion of Ammonium Perchlorate-Based Composite Propellants: A discussion of Some Recent Experimental Results, Ministry of Aviation, E.R.D.E. Report No. 15/R/65, October 1965
5. L. A. Dickinson, E. L. Capener, R. J. Kier, Research on Unstable Combustion in Solid Propellant Rockets, Annual Report, 1 January - 31 December 1964, Contract No. AF 49(638)-1367, Stanford Research Institute Project No. 4865
6. E. L. Capener, L. A. Dickinson, and G. A. Marxman, Propellant Combustion Phenomenon During Rapid Depressurization, 1st Quarterly Progress Report, Contract NAS7-389, October 12, 1965
7. J. Sotter, Chemical Kinetics of the Cordite Explosion Zone, Tenth Symposium (International) on Combustion, pp. 1405-1411, The Combustion Institute, 1965
8. E. W. Price, Review of the Combustion Instability Characteristics of Solid Propellants, presented at the 25th Meeting of AGARD Combustion and Propulsion Panel, San Diego, California, 22-24 April 1965
9. M. D. Horton, and E. W. Price, Dynamic Characteristics of Solid Propellant Combustion, Ninth Symposium on Combustion, pp. 303-310, The Combustion Institute, 1963
10. J. Powling, and W. A. W. Smith, Measurement of the Burning Surface Temperatures of Propellant Compositions by Infrared Emission, *Combustion and Flame* 6, 173 (1962)
11. J. Powling, and W. A. W. Smith, The Surface Temperature of Ammonium Perchlorate Burning at Elevated Pressures, Tenth Symposium (International) on Combustion, pp. 1373-1380, The Combustion Institute, 1965

REFERENCES (Concluded)

12. B. B. Goshgarian, and J. A. Walton, Mass Spectrometric Study of Ammonium Perchlorate Decomposition, Report No. AFRPL-TR-65-87, Air Force Rocket Propulsion Laboratory, Edwards, California, April 1965
13. L. A. Dickinson, and F. Jackson, Combustion in Solid Propellant Rocket Engines, 5th AGARD Colloquium on Combustion and Propulsion, The Macmillan Company, New York, 1963, pp. 531-550
14. G. von Elbe, Theory of Solid Propellant Ignition and Response to Pressure Transients, Bulletin of the 18th ICRPG Meeting (1963), p. 95
15. L. C. Landers, et al., Development of an Extinguishable Solid Propellant (U), Aerojet General Report No. 0855-81Q-2, 23 October 1964 (CONFIDENTIAL)
16. D. A. Bittker, An Analytical Study of Turbulent and Molecular Mixing in Rocket Combustion, NASA TN 4321-1958
17. M. R. Denison, and E. Baum, A Simplified Model of Unstable Burning in Solid Propellants, ARS Journal 31, 1112 (1961)
18. M. Imber, Transient Effects in Solid Propellant Burning, AIAA J., Vol. 3, No. 5, p. 890, May 1965

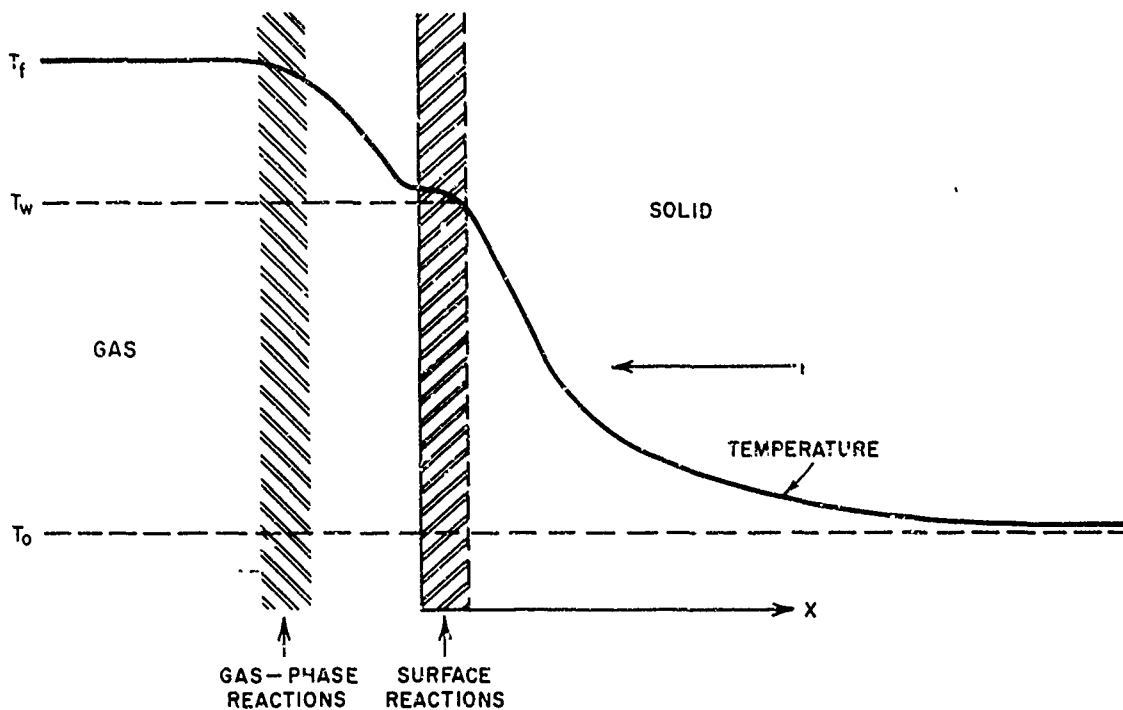
Appendix A

SIMPLIFIED MODEL OF UNSTEADY COMBUSTION IN SOLID PROPELLANTS

Denison and Baum¹⁷ have considered a simplified model of propellant combustion in which it was assumed (a) that gas-phase reactions can be represented in terms of a single reaction of arbitrary order that obeys Arrhenius kinetics and responds with negligible time lag to pressure disturbances; (b) that there is no erosive burning; (c) that the Lewis number is unity in the gas phase; (d) that surface vaporization follows an Arrhenius law; and (e) that there are no solid-phase reactions. Their perturbation analysis determined the response of this model combustion process, initially burning in steady state, to a sudden oscillation or step-change in pressure, and derived stability criteria in terms of thermochemical parameters of the propellant. Recently this analysis was extended by Imber,¹⁸ using the same combustion model, to include the possibility of a time-varying temperature profile in the grain prior to the pressure perturbation, as during ignition; corresponding modifications in the stability criteria were derived. The basic approach taken in these analyses is commendable, but the results probably are of limited value owing to the rather unrealistic combustion model, which omits what may be key steps in the combustion mechanism.

To develop an improved theory of unsteady combustion, it seems desirable to retain the general approach of the perturbation analyses, while employing a less restrictive combustion model.

We recognize that any model must allow for the presence of solid-phase reactions and ultimately for situations in which gas-phase relaxation times may not be negligible, perhaps as in surface-coupled gas-phase reactions. Accordingly, as a first step in developing an improved model we shall consider the combustion model of Fig. A-1, in which exothermic (or endothermic) reactions are permitted within the solid phase, at or very near the interface. In this idealized model these solid-phase reactions will be assumed to occur in a surface layer of negligible thickness relative to the penetration depth of the temperature profile.



TA-5577-6

FIG. A-1 COMBUSTION MODEL WITH GAS PHASE AND SOLID PHASE REACTION

This assumption greatly simplifies the mathematical analysis and is entirely consistent with the simple Arrhenius kinetics employed to describe the reaction processes.

The equation governing heat conduction in the solid phase beyond the surface reaction zone is (see section on Nomenclature for definition of symbols):

$$\frac{\partial T}{\partial t} = r(t) \frac{\partial T}{\partial x} + K \frac{\partial^2 T}{\partial x^2} \quad (1)$$

The vaporization process at the wall is assumed to follow an Arrhenius law so that the burning rate is related to wall temperature as follows:

$$r = a \exp(-E/RT_w) \quad (2)$$

The following boundary condition is imposed upon the temperature:

$$x \rightarrow \infty; \quad T \rightarrow T_0 \quad (3)$$

The remaining boundary condition is obtained through an energy-flux balance at the solid-gas interface. The net heat conducted into the

unreacted solid propellant from the interface at the plane $x = 0$ is:

$$-k \left(\frac{\partial T}{\partial x} \right)_w = -k \left(\frac{\partial T}{\partial x} \right)_{g_w} - \rho_s r h_{g_w} + \rho_s r h_{s_w} + Q_H + Q_D \quad (4)$$

The first term on the right-hand side of the equality sign represents the energy coming from the gas-phase; the second, the energy carried into the gas with the vaporizing propellant; the third, the energy carried by convection from the unreacted solid phase into the interface; the fourth, the energy released (positive) in heterogeneous decomposition reactions at the surface whose reaction rates depend upon the local gas-phase density; and the last, the energy released in solid-phase surface reactions with rates that are independent of gas-phase conditions. It is convenient to rewrite this expression as follows:

$$-k \left(\frac{\partial T}{\partial x} \right)_w = -k \left(\frac{\partial T}{\partial x} \right)_{g_w} + \rho_s r [(C_s - C_p) T_w - L] + Q_H + Q_D \quad (5)$$

Denison and Baum²⁰ have obtained a solution to the gas-phase conservation equations by assuming that the complex gaseous reaction process can be represented by a single-step reaction of order n , where in some cases n may not be an integer. For now we shall retain their gas-phase solution, which yields the following expression for the heat flux from the gas phase to the wall:

$$-k \left(\frac{\partial T}{\partial x} \right)_{g_w} = \rho_s r [\epsilon_r Q_r - C_p (T_f - T_w)] \quad (6)$$

This solution also relates the instantaneous flow of reactant into the gaseous reaction zone, $\rho_s r$, to the instantaneous gas-phase reaction rate, so that:

$$r = C_p T_f^{\frac{n}{2} \frac{n}{2} + 1} \exp(-E_f/2RT_f) \quad (7)$$

Heterogeneous decomposition reactions at the interface will proceed at a rate proportional to the total mass flux through the surface reaction zone, $\rho_s r$. The fraction of this material involved in the heterogeneous reaction depends upon the density of the gas-phase reactant and on the

Arrhenius law of the reaction. Thus:

$$Q_H = \rho_s r H_H \left(\frac{P}{T_w} \right)^m \exp(-E_H/RT_w) \quad (8)$$

Except that they are independent of the gas-phase density at the surface, the other decomposition reactions (represented here as a single step reaction, consistent with the gas-phase treatment) follow a similar law:

$$Q_D = \rho_s r H_D \exp(-E_D/RT_w) \quad (9)$$

Equations (5), (6), (8), and (9) can be combined to obtain:

$$-k \left(\frac{\partial T}{\partial x} \right)_w = \rho_s r \left[\epsilon_r Q_r - L - C_p T_f + C_s T_w + H_H \left(\frac{P}{T_w} \right)^m \exp(-E_H/RT_w) + H_D \exp(-E_D/RT_w) \right] \quad (10)$$

Equations (1), (2), and (7), with the boundary conditions of Eqs. (3) and (10), complete the mathematical representation of the combustion model in terms of the dependent variables T_f , T_w , and r . Owing to the nonlinear character of these equations, a closed-form solution cannot usually be obtained. Consequently, to avoid unwarranted numerical calculation, we resort to a small-perturbation analysis, assuming that each dependent variable, as well as the pressure, is the sum of a steady and a perturbed component:

$$\begin{aligned} P &= \bar{P}(1 + \tilde{P}) \\ T_f &= \bar{T}_f(1 + \tilde{T}_f) \\ T_w &= \bar{T}_w(1 + \tilde{T}_w) \\ r &= \bar{r}(1 + \tilde{r}) \end{aligned} \quad (11)$$

where, for example, \tilde{P} is the ratio $\frac{P(t) - \bar{P}}{\bar{P}} \ll 1$. By introducing these expressions into Eqs. (1), (2), (3), (7), and (10), and retaining only first-order terms in the perturbed quantities, one can obtain a set of linear equations. The solution to these equations gives the first-order response of the combustion mechanism to a perturbation in the chamber pressure.

Denison and Baum¹⁷ and Imber¹⁸ have carried out such a solution for their simple combustion model, in which solid-phase exothermic or endo-

thermic reactions are not permitted. In future work it will be shown that the present problem, in which such reactions are allowed, can be made mathematically identical to that of the simpler model by suitably redefining certain parameters. This permits the use of earlier results, obtained from a rather complicated analysis, to determine the response of the present combustion model to pressure perturbations.

An Approximate Solution

Before developing a precise solution, it may be instructive to obtain an approximate solution corresponding to the present combustion model. The mathematical complexity of the problem can thereby be greatly reduced, which should facilitate a physical interpretation of the results.

With this objective in mind, let us integrate Eq. (1) over x to obtain:

$$\frac{\partial}{\partial t_0} \int_0^{\infty} (T - T_0) dx = -r(t_w - t_0) - K \left(\frac{\partial \theta}{\partial x} \right)_w \quad (12)$$

To evaluate the integral, which represents essentially the total energy stored in the grain at any instant, it is convenient to assume a steady-state temperature profile,

$$T - T_0 = (T_w - T_0) \exp^{-rx/K} \quad (13)$$

As rapid changes appear in the heat flux, the temperature profile shape will reflect the corresponding small changes in surface temperature much more readily than it will respond to the much larger simultaneous changes in burning rate. Thus, for purposes of the approximate analysis, dT/dr will be neglected. Then Eq. (12) becomes:

$$\frac{K}{r} \frac{dT_w}{dt} = -r(T_w - T_0) - K \left(\frac{\partial T}{\partial x} \right)_w \quad (14)$$

It is worth digressing briefly to note that the assumptions leading from Eq. (12) to Eq. (14) do not reduce the present analysis to a quasi-steady treatment comparable to those discussed in the text of this report. Here the surface temperature has been allowed to vary, and the primary

transient in the temperature profile has been considered. Moreover, the possible shift in relative importance of solid- and gas-phase reactions under transient conditions is accounted for in the present approach, as no empirical burning rate law is used.

Equations (11) can now be substituted into Eqs. (2), (7), (10), and (14), and terms of equal order collected. Terms of the order of \bar{P} (or \bar{T}_f , \bar{T}_w , \bar{r}) comprise the unperturbed equations, while those of the order of \tilde{P} form the linearized mathematical description of the response to pressure perturbations.

Combustion Without Pressure Disturbances

The equations for undisturbed burning of the solid propellant are:

$$\bar{r} = a \exp(-E/RT_w) \quad (15)$$

$$\bar{r} = C_P \bar{T}_f^{\frac{n}{2} + 1} \exp(-E_f/RT_f) \quad (16)$$

$$\frac{K}{r^2} \frac{d\bar{T}_w}{dt} = T_0 + \frac{\epsilon_r Q_r}{C_s} - \frac{L}{C_s} - \frac{C_P \bar{T}_f}{C_s} + \frac{H_H}{C_s} \exp(-E_H/RT_w) \left(\frac{\bar{P}}{\bar{T}_w}\right)^m + \frac{H_D}{C_s} \exp(-E_D/RT_w) \quad (17)$$

These equations are nonlinear, and, except by numerical methods, no solution can be readily obtained. A numerical solution, if obtained, would describe the "normal" behavior of the combustion process, i.e., the behavior in the absence of disturbances caused, for example, by acoustical interactions in the chamber. The steady state solution ($d\bar{T}_w/dt = 0$) would correspond, within the limitation of the model, to the behavior usually described in terms of an empirical law such as $r = bP^n$.

The First-Order Response to Pressure Perturbations

The first-order response of the combustion model to pressure transients is obtained by collecting terms of the order of ratios of perturbed to unperturbed quantities, i.e., \tilde{P} , \tilde{r} , \tilde{T}_w , and \tilde{T}_f . Coefficients in these equations may be simplified by appropriate substitutions from Eqs. (15),

(16), and (17). After considerable algebraic manipulation, one obtains the following set of linear equations:

$$\tilde{r} = \frac{E}{RT_w} \tilde{T}_w \quad (18)$$

$$\tilde{T}_f = \frac{\frac{E}{RT_w} \tilde{T}_w - \frac{n}{2} \tilde{P}}{\Sigma} \quad (19)$$

where

$$\Sigma = \frac{n+2}{2} + \frac{E_f}{2RT_f}$$

$$\begin{aligned} \frac{K}{r^2} \frac{\partial \tilde{T}_w}{\partial t} = & \left[-\frac{K}{r^2} \left(\frac{\partial \bar{T}}{\partial t} \right)_w \frac{1}{\bar{T}_w} + \theta_H \left(\frac{E_H}{RT_w} - m \right) + \theta_D \frac{E_D}{RT_w} \right] \tilde{T}_w \\ & - \left[4 \left(\frac{\bar{T}_w - T_0}{\bar{T}_w} \right) + \frac{1}{\bar{T}_w} \frac{K}{r^2} \frac{\partial \bar{T}_w}{\partial t} \right] \tilde{r} - r^2 \frac{C_P}{C_S} \frac{\bar{T}_f}{\bar{T}_w} \tilde{T}_f + r^2 \frac{\theta_H^m}{\bar{T}_w} \tilde{P} \end{aligned} \quad (20)$$

where

$$\theta_H = \frac{H_H}{C_S \bar{T}_w} \exp(-E_H/RT_w) \left(\frac{\bar{P}}{\bar{T}_w} \right)^m; \quad \theta_D = \frac{H_D}{C_S \bar{T}_w} \exp(-E_D/RT_w)$$

It is convenient to combine these equations to obtain the following differential equation for \tilde{r} :

$$\frac{d\tilde{r}}{dt} - C_1 \tilde{r} = C_2 \tilde{P} \quad (21)$$

where

$$C_1 = \frac{r^2}{K} \left[\theta_H \left(\frac{E_H}{RT_w} - m \right) + \theta_D \frac{E_D}{RT_w} - \frac{C_P}{C_S} \frac{\bar{T}_f}{\bar{T}_w} \frac{E/RT_w}{\Sigma} + \frac{K}{\bar{T}_w r^2} \left(\frac{2E}{RT_w} - 1 \right) \left(\frac{\partial \bar{T}}{\partial t} \right)_w \right] \quad (22)$$

$$C_2 = \frac{\bar{r}^2}{K} \frac{E}{RT_w} \left[\theta_{H^m} + \frac{n}{2} \frac{C_p}{C_s} \frac{\bar{T}_f}{T_w} \frac{1}{\Sigma} \right] \quad (23)$$

Response to Sinusoidal Pressure Oscillations or an Exponential Pressure Decay; A Stability Criterion

An oscillatory perturbation in the chamber pressure can be expressed as:

$$\tilde{P} = \epsilon \sin \omega t \quad (24)$$

where the ratio of the oscillation amplitude to the steady-state pressure is $\epsilon \ll 1$. The corresponding solution to Eq. (21), assuming $\tilde{r} = 0$ at $t = 0$, is:

$$\tilde{r} = \frac{C_2}{C_1^2 + \omega^2} \left[\omega \exp^{C_1 t} - C_1 \sin \omega t - \omega \cos \omega t \right] \quad (25)$$

The chamber-pressure decay introduced within the port of a solid rocket to terminate combustion typically has the form:

$$\tilde{P} = \exp^{-\beta t} - 1 \quad (26)$$

(Note that at $t = 0$, $d\tilde{P}/dt = -\beta$, $\frac{d\tilde{r}}{dt} = -\beta\bar{r}$.) From Eq. (21), the approximate initial response of the burning rate to this pressure decay is:

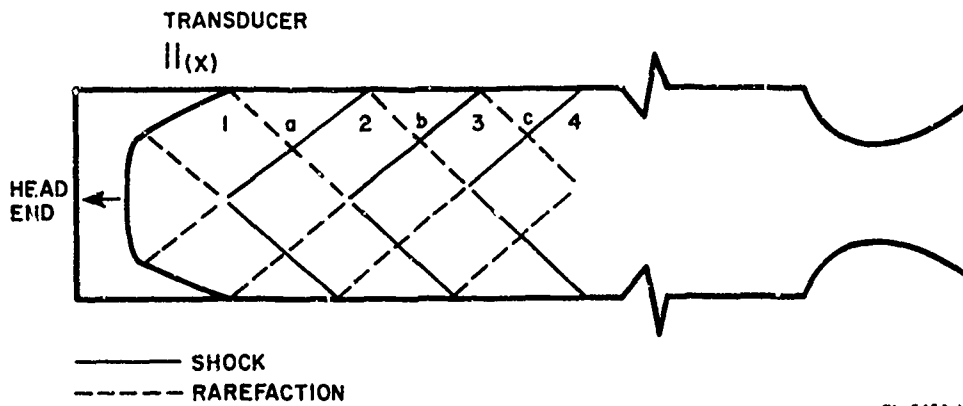
$$\tilde{r} = \frac{C_2}{\beta + C_1} (\exp^{C_1 t} - \exp^{-\beta t}) + \frac{C_2}{C_1} (1 - \exp^{C_1 t}) \quad (27)$$

Appendix B

REFLECTION OF TRAVELING PRESSURE WAVES AT THE ENDS OF THE COMBUSTION CHAMBER

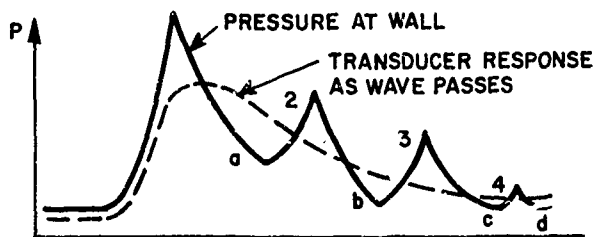
The general character of the traveling wave phenomena observed in axial instability studies is worthy of further consideration, particularly the reflection process at the chamber ends. As shown in Fig. B-1, the pressure transducer records indicate that the amplitude of a pressure pulse initiated at one end of the motor tends to grow continuously as the wave passes through the chamber during unstable operation. This, of course, corresponds to the transfer of energy from the combustion process to the pressure wave, which is implicit in an unstable combustion phenomenon. More difficult to explain, and probably of greater importance in many respects, is the end-wall wave reflection observed in axially unstable motors.

This reflection is strikingly different from that in a shock tube, for example. In the latter a plane shock, moving into a region at pressure p_1 , and followed by a region at p_2 , where $p_2 > p_1$, ultimately reflects from the end wall with approximately the same strength, re-entering the zone it has just left at pressure p_2 . Thus, the pressure behind the reflected shock is p_3 , where $p_3/p_2 \approx p_2/p_1$. In this way the well-known "pressure doubling" behind the reflected wave in a shock tube is achieved. Note that the pressure behind the original shock remains at p_2 until the reflected shock arrives, and the pressure in the zone behind the latter remains at p_3 until the arrival of a reflected rarefaction wave from the other end of the tube. In other words, the traveling pressure pulse, or shock, in a shock tube is not followed by an immediate pressure decay, as in the combustion chamber of a solid rocket motor. Moreover, the pressure wave in the rocket motor reflects from the end wall with a somewhat diminished amplitude, in marked contrast to the pressure doubling in shock tubes. It is apparent that these two traveling wave phenomena are fundamentally different when viewed from the standpoint of the gasdynamics of the cavity.



TA-5456-19

FIG. B-1(a) VISUALIZATION OF SHOCK WAVE STRUCTURE BEHIND TRAVEL SHOCK FRONT IN ROCKET MOTOR B



TA-5456-19a

FIG. B-1(b) VISUALIZATION OF TRANSDUCER RESPONSE AT STATION X

An examination of the probable effect of the combustion process and mass addition on the shape of the pressure front (or shock) moving through the rocket chamber affords a plausible explanation for this difference. In the rocket chamber there is a very sharp temperature gradient between the propellant surface and main gas-phase reactions just above that surface, followed by a less steep gradient a little farther from the surface as the reactions go to completion. Consequently, the velocity of sound, to which the pressure-wave velocity is closely related, though a little higher, is much higher near the center of the chamber than at the propellant surface. Also, there is a strong convective flux normal to the surface. Together these characteristics would be expected to distort the shock shape substantially, with a resulting profile that probably is similar to the qualitative representation in Fig. B-1.

In the central part of the chamber, where the temperature is high and nearly uniform, the shock speed tends to be higher than near the wall, where the temperature is lower and changing. As the wave proceeds down the port this results in a shock profile such as that depicted as "1" in Fig. B-1(a). Therefore, at the propellant surface the shock is essentially oblique in character, and the flow is turned away from the surface in the region behind the shock. Thus a rarefaction wave is formed as indicated by the dashed line a. This sequence is repeated several times as shown, with each shock and subsequent rarefaction weaker than the preceding set. The resulting instantaneous pressure distribution along the propellant is shown in the upper part of the figure; this also represents the pressure vs. time plot for a given point on the surface as the pressure pulse passes over that point. Owing to the very short time between pressure peaks, the response of a pressure transducer in the wall would tend to be more smooth, as indicated. Clearly the concept of a curved shock profile is consistent with the type of pressure pulse that has been observed experimentally.

The reflection process provides a second test of this idea. Note that as the oblique portion of the shock near the wall is reflected, it enters the approaching rarefaction zone behind a almost at once. In

other words, the reflected shock enters a zone of reduced pressure, which is entirely different from the situation in a shock tube. Following the reflection of the entire curved shock (or shock train), one can see that the reflected pressure pulse will have about the same shape as the original one, and an equal or lower amplitude (with some losses at the end wall inevitable). Again, this conclusion is consistent with experimental observations.

In summary, it appears that a pressure front moving down a combustion chamber has a strong tendency to assume a sharply curved surface, and that if we assume this to be true the major features of the experimental results can be explained, at least qualitatively. Further experiments are planned to ascertain the validity of this concept and to better define the details of the traveling wave phenomenon.

Unclassified
Security Classification

DOCUMENT CONTROL DATA - R&D		
<i>(Security classification of title, body of abstract and indexing annotation must be entered when the overall report is classified)</i>		
1 ORIGINATING ACTIVITY (Corporate author)		2a REPORT SECURITY CLASSIFICATION
Stanford Research Institute <i>Menlo Park, California</i>		UNCLASSIFIED
3 REPORT TITLE		2b GROUP
RESPONSE OF A BURNING PROPELLANT SURFACE TO EROSION TRANSIENTS		
4 DESCRIPTIVE NOTES (Type of report and inclusive dates)		
Final Scientific Report - January 1 - December 31, 1965		
5 AUTHOR(S) (Last name, first name, initial)		
Capener, E. L., L. A. Dickinson, R. J. Kier, and G. A. Marxman		
6 REPORT DATE	7a TOTAL NO. OF PAGES	7b NO OF REFS
March 15, 1966	92	18
8a CONTRACT OR GRANT NO.	9a ORIGINATOR'S REPORT NUMBER(S)	
AF 49(638)-1507		
b PROJECT NO		
<i>9713-01</i>		
ORR Project No. PRU 5458		
c	9b. OTHER REPORT NO(S) (Any other numbers that may be assigned <i>is report</i>)	
61445014	AFOSR 66-0885	
10 AVAILABILITY/LIMITATION NOTICES		
Distribution of this document is unlimited		
11 SUPPLEMENTARY NOTES	12. SPONSORING MILITARY ACTIVITY	
	Air Force Office of Scientific Research Washington, D. C. 20333	
13 ABSTRACT		
<p>An experimental and theoretical study of finite amplitude axial mode instability has shown that instability is associated with significant heat release in the solid-phase-coupled reactions. In general ammonium perchlorate-based composite propellants are unstable at elevated pressures while double base propellants are unstable at low pressures.</p> <p>Studies of wave propagation show that reflection of the waves at the ends of the motor is associated with severe energy loss and high heat transfer.</p> <p>A generalized theoretical approach toward determining the response of propellant to pressure perturbation is outlined. In the case of composite propellants approaches in propellant selection are indicated as a means of avoiding axial mode instability.</p>		

DD FORM 1473
1 JAN 64

Unclassified
Security Classification

14	KEY WORDS	LINK A		LINK B		LINK C	
		ROLE	WT	ROLE	WT	ROLE	WT
Combustion instability (U) Axial mode (U) Composite propellants (U) Heat transfer (U)							

INSTRUCTIONS

1. **ORIGINATING ACTIVITY:** Enter the name and address of the contractor, subcontractor, grantee, Department of Defense activity or other organization (*corporate author*) issuing the report.
- 2a. **REPORT SECURITY CLASSIFICATION:** Enter the overall security classification of the report. Indicate whether "Restricted Data" is included. Marking is to be in accordance with appropriate security regulations.
- 2b. **GROUP:** Automatic downgrading is specified in DoD Directive 5200.10 and Armed Forces Industrial Manual. Enter the group number. Also, when applicable, show that optional markings have been used for Group 3 and Group 4 as authorized.
3. **REPORT TITLE:** Enter the complete report title in all capital letters. Titles in all cases should be unclassified. If a meaningful title cannot be selected without classification, show title classification in all capitals in parenthesis immediately following the title.
4. **DESCRIPTIVE NOTES:** If appropriate, enter the type of report, e.g., interim, progress, summary, annual, or final. Give the inclusive dates when a specific reporting period is covered.
5. **AUTHOR(S):** Enter the name(s) of author(s) as shown on or in the report. Enter last name, first name, middle initial. If military, show rank and branch of service. The name of the principal author is an absolute minimum requirement.
6. **REPORT DATE:** Enter the date of the report as day, month, year, or month, year. If more than one date appears on the report, use date of publication.
- 7a. **TOTAL NUMBER OF PAGES:** The total page count should follow normal pagination procedures, i.e., enter the number of pages containing information.
- 7b. **NUMBER OF REFERENCES:** Enter the total number of references cited in the report.
- 8a. **CONTRACT OR GRANT NUMBER:** If appropriate, enter the applicable number of the contract or grant under which the report was written.
- 8b, c, & 8d. **PROJECT NUMBER:** Enter the appropriate military department identification, such as project number, subproject number, system numbers, task number, etc.
- 9a. **ORIGINATOR'S REPORT NUMBER(S):** Enter the official report number by which the document will be identified and controlled by the originating activity. This number must be unique to this report.
- 9b. **OTHER REPORT NUMBER(S):** If the report has been assigned any other report numbers (*either by the originator or by the sponsor*), also enter this number(s).
10. **AVAILABILITY, LIMITATION NOTICES:** Enter any limitations on further dissemination of the report, other than those

imposed by security classification, using standard statements such as:

- (1) "Qualified requesters may obtain copies of this report from DDC."
- (2) "Foreign announcement and dissemination of this report by DDC is not authorized."
- (3) "U. S. Government agencies may obtain copies of this report directly from DDC. Other qualified DDC users shall request through _____."
- (4) "U. S. military agencies may obtain copies of this report directly from DDC. Other qualified users shall request through _____."
- (5) "All distribution of this report is controlled. Qualified DDC users shall request through _____."

If the report has been furnished to the Office of Technical Services, Department of Commerce, for sale to the public, indicate this fact and enter the price, if known.

11. **SUPPLEMENTARY NOTES:** Use for additional explanatory notes.

12. **SPONSORING MILITARY ACTIVITY:** Enter the name of the departmental project office or laboratory sponsoring (*paying for*) the research and development. Include address.

13. **ABSTRACT:** Enter an abstract giving a brief and factual summary of the document indicative of the report, even though it may also appear elsewhere in the body of the technical report. If additional space is required, a continuation sheet shall be attached.

It is highly desirable that the abstract of classified reports be unclassified. Each paragraph of the abstract shall end with an indication of the military security classification of the information in the paragraph, represented as (TS), (S), (C) or (U).

There is no limitation on the length of the abstract. However, the suggested length is from 150 to 225 words.

14. **KEY WORDS:** Key words are technically meaningful terms or short phrases that characterize a report and may be used as index entries for cataloging the report. Key words must be selected so that no security classification is required. Identifiers, such as equipment model designation, trade name, military project code name, geographic location, may be used as key words but will be followed by an indication of technical context. The assignment of links, rules, and weights is optional.